Semi-Empirical Tight-Binding
Ways and Means for the Atomistic Simulation of Materials

Von der Gemeinsamen Naturwissenschaftlichen Fakultät
der Technischen Universität Carolo-Wilhelmina
zu Braunschweig
zur Erlangung des Grades eines
Doktors der Naturwissenschaften
(Dr.rer.nat)
genehmigte
`Dissertation`

von Oliver Hein
aus Glückstadt

1. Referent: Prof. Dr. von Niessen

2. Referent: Prof. Dr. Becker

eingereicht am: 23.09.1999

mündliche Prüfung (Disputation) am: 17.12.1999

Druckjahr 2000

Vorveröffentlichungen der Dissertation

Teilergebnisse aus dieser Arbeit wurden mit Genehmigung der Gemeinsamen Naturwissenschaftlichen Fakultät, vertreten durch den Mentor, im folgenden Beitrag vorab veröffentlicht:

Publikationen

1. H. Dücker, **O. Hein,** S. Knief, W. von Niessen, Th. Koslowski
   Theoretical approaches to the electronic structure of disordered solids
   Journal of Electron Spectroscopy and Related Phenomena 1 (1999), in press

Dedicated to my parents

Acknowledgements. I am very grateful to my supervisor Professor Dr. von Niessen, who accepted me as a, not always easy to handle, student, provided me with excellent scientific guidance, and intensive discussions over a period of four years. I am especially grateful for the freedom to let me go my own way.

Sincere thanks are also given to Prof. Becker for co-referencing this work.

I also would like to thank my colleague Dr. O. Kortlüke for offering me great assistance in computer knowledge.

Contents

Zusammenfassung

Bedingt durch die technologischen Entwicklungen im Bereich der Nanotechnologie ist in den letzten Jahren ein stetig wachsendes Interesse an sowohl quantenmechanischen als auch klassischen Rechnungen, wie sie z.B. Molekulardynamik Simulationen darstellen, zu beobachten. Für den theoretisch arbeitenden Chemiker oder Physiker stellen die mesoskopischen Systeme eine hohe Herausforderung dar, da sie zum einen von hoher praktischer und wirtschaftlicher Bedeutung sind und zum anderen eine Komplexität aufweisen, die praktische Berechnungen in den Bereich des Möglichen rückt. Dies gilt um so mehr, als es die rasante Entwicklung auf dem Soft- sowie Hardwaresektor immer leichter macht, anspruchsvolle Simulationen in einem sowohl zeitlich als auch finanziell akzeptablem Rahmen durchzuführen. Die vorliegende Arbeit hat es sich zum Ziel gesetzt, eine Software zu entwickeln, welche es sowohl dem Theoretiker, aber auch dem im Labor arbeitenden Praktiker, ermöglichen soll, derartige Rechnungen durchzuführen.

Als theoretische Grundlage dient hierbei die tight-binding Methode, die als die Festkörperadaption der wohlbekannten LCAO-Methode der theoretischen Chemie aufgefasst werden kann (Kapitel 2). Um im Rahmen dieser Methode die Bandstruktur und Zustandsdichte einer kristallinen Substanz berechnen zu können, muss die der Struktur der Substanz entsprechende Hamiltonmatrix aufgestellt werden. Wie sich nun aber leider zeigt, ist das Aufstellen dieser Matrix für ein simples System, wie es z.B. Silizium darstellt, zwar eine triviale Sache, aber für komplexere Systeme, wie z.B. monoklines TiO mit Fehlstellen, hingegen eine von Hand nicht mehr durchführbare Aufgabe. In der gegenwärtigen Literatur werden demzufolge auch nur strukturell

sehr einfach aufgebaute Systeme, vornehmlich solche mit kubischer, Diamant- oder Zinkblendestruktur, behandelt. Das in dieser Arbeit entwickelte Programmpaket ist entgegen dem konventionellen Ansatz völlig allgemeingültig konzipiert. Es entwickelt den Hamiltonoperator auf der Grundlage der allgemeinen Struktur, d.h. Bravais Gitter plus Basis, für ein beliebiges System, unabhängig von dessen Komplexität (Kapitel 2). Die Philosophie der Software ist dabei ausgerichtet auf Erweiterbarkeit und einfache Bedienbarkeit. Dies bedeutet einen streng modularen Aufbau, sowie die Steuerung der einzelnen Module durch eine grafische Benutzeroberfläche. Es ist evident, dass eine derartige Allgemeingültigkeit und Bedienfreundlichkeit nur auf Kosten des Programmieraufwands erreichbar ist. Dieser rechtfertigt sich aber spätestens dann, wenn komplexere Systeme als solche mit Kochsalz oder Zinkblendestruktur in Angriff genommen werden sollen. Derartige komplexe Strukturen sind in der Praxis nicht die Ausnahme, sondern eher die Regel, wie schon ein Blick auf die momentan hoffnungsvollsten Vertreter im Bereich der Supraleitung zeigt.

Ein zweiter wesentlicher Punkt neben der Struktur ist die Wahl der tight-binding Parameter. Wünschenswert wäre hier ein genereller Satz von Parametern für alle Elemente des Periodensystems, welcher die Beschreibung einer beliebigen Verbindung zuliesse. Der in diese Richtung gehende Ansatz von Harrison wird im zweiten Kapitel untersucht. Es zeigt sich dabei, dass der Parametersatz von Harrison, angewendet auf verschiedene Verbindungen, lediglich ein grobes, qualitatives Bild der Substanz liefert. Eine quantitativ korrekte Beschreibung ist nicht möglich. Es ist im Gegenteil so, dass der benötigte tight-binding Parametersatz für jede Substanz speziell erarbeitet werden muss. In der Literatur sind viele Beispiele für derartige spezielle Parametersätze angegeben. Leider zeigt es sich hierbei aber allzu häufig,

dass die in der älteren Literatur gegebenen Parametersätze zwar die exzellente Reproduktion einer mit ab initio Methoden berechneten Bandstruktur ermöglichen, sie aber einfachsten sinnvollen Annahmen über das Vorzeichen und das Skalenverhalten von Matrixelementen widersprechen. Die Ursache ist im Aufsuchen dieser Parameter zu sehen. Die Parameter werden durch ein Fitverfahren gefunden, welches den Abstand der tight-binding Bandstruktur oder DOS im Sinne einer Norm von einer Zielfunktion an ausgesuchten Fitpunkten minimiert. Nun ist allerdings der Parameterraum sehr gross (über 100 Parameter sind keine Seltenheit) und das Fitproblem ist nichtlinearer Natur. Um es zu lösen, bedarf es einer guten Kenntnis des Parameterraums (hier ist insbesondere die Wahl des Startvektors zu nennen) und der Eigenschaften des Fitalgorithmus. Alles Dinge, die dem erfahrenen Anwender vorbehalten sind. Und selbst diesem ist es dann nicht immer möglich, konsistente Parametersätze anzugeben. Um eine Verbesserung in Bezug auf diese Tatsachen zu erreichen, wird in der vorliegenden Arbeit im dritten Kapitel ein Fitalgorithmus auf der Grundlage des simulated annealing vorgestellt und untersucht. Dieser Algoritmus ist stark genug, den Parameterraum in seiner ganzen Weite und in adäquater Zeit nach geeigneten, physikalisch sinnvollen, Werten zu durchsuchen.

Im vierten Kapitel der Arbeit wird gesondert auf die Vorzeichen und besonders die Skalengesetze der Matrixelemente eingegangen. Für diese existieren in der neuesten Literatur eine Reihe von unterschiedlichen Vorschlägen. Es wird untersucht, in wie weit man diese Skalengesetze verallgemeinern und abschwächen kann und immer noch physikalisch sinnvolle Ergebnisse erhält. Dies ist notwendig, um die Universalität der Software sicherzustellen. Es zeigt sich, dass die zu fordernden Restriktionen erstaunlich gering sind. Nur die Vorgabe der richtigen Vorzeichen und eines rein qualitativen Skalen-

gesetzes führt zu qualitativ hochwertigen Ergebnissen. Diese Erkenntnis ist um so bemerkenswerter, wenn man noch die benötigte Menge an Eingangsinformation in Betracht zieht. Als Eingabe sind nur sehr wenige Energiewerte ausreichend, welche direkt aus spektroskopischen Befunden gewonnen werden können.

Um in der Arbeit den Anschluss und die Vergleichbarkeit mit anderen Verfahren und Ansätzen zu gewährleisten, wurde vornehmlich das Beispiel Silizium behandelt. Dieses stellt in der Literatur, zusammen mit Kohlenstoff, das im Kontext des vorliegenden Ansatzes am besten untersuchte System dar.

Ein im Rahmen dieser Arbeit nicht dargestellter aber in die Software implementierter Teil, befasst sich mit in der schnellen und stabilen numerischen Bestimmung der DOS. Es wurde dazu ein Algorithmus implementiert, welcher linear mit der Anzahl der Atome skaliert und in seinem Kern in parallelisierter Form vorliegt. Dieser Algorithmus ist ein weiterer wichtiger Schritt in Richtung auf die Berechenbarkeit mesoskopischer Systeme.

Auf Grund der Untersuchungen zeigt sich, dass die tight-binding Methodik als konzeptionelle Grundlage, im Zusammenspiel mit den modernen Verfahren der Optimierung und Numerik, sowie der rasanten Entwicklung der Soft- und Hardware, ein möglicher Zugangsweg zum qualitativen und quantitativen Verständnis der kondensierten Materie darstellt. Als Stichwörter seien hier chemical engineering und material science genannt, welche in den kommenden Jahren in ihrer Bedeutung weiter wachsen und wahrscheinlich einen wesentlichen Wirtschaftsfaktor ausmachen werden.

Chapter 1

Introduction

The last few years have seen a growing interest in the properties of substances on a mesoscopic length scale. This interest is mainly driven by the progress of miniaturization in the field of electrical engineering. To make present day computers more and more powerful, it is essential to make the circuits ever smaller. The next generation of devices will reach a level of miniaturization, which trespasses the length scale from where on quantum mechanical phenomena become relevant. These quantum mechanical phenomena are not necessarily obstacles for progress, but also represent ways and means to create new devices, with properties yet unknown. This is also true for a growing number of new substances, whose astonishing properties rest upon their mesoscopic structure, e.g., fullerenes, bucky paper, etc. [74], [24], [28], [63]. It is the objective of chemical/material engineering to understand and than to manipulate these substances/devices to give them new and useful properties. To do so, it is mandatory to be able to perform quantum mechanical computations in the mesoscopic region, i.e., at least in the region of $10^6 - 10^{12}$ atoms.

Investigating the electronic and magnetic properties of a solid can be re-

garded in principle from two different viewpoints. As a pure theoretician, one will try to derive all the interesting features of the material under investigation by solving the fundamental equations of physics. This is to say that one tries to solve the Schrödinger equation without any assumptions in the form of fitted parameters. While very satisfactory from a philosophical point of view, the disadvantage is that this approach does not work for substances, which are significantly more complex than hydrogen. In the real world, however, more complex materials are the ones, which are of relevance for basic research on complex phenomena and for industry. Thus one has to fall back on different approximations, which in turn implies to a certain degree fitting to empirical data. In the extreme limit one could fit an empirical data set to a numerically convenient fitting function, e.g., a polynomial, and then extrapolate the function into the unknown region, with the hope that the fit function can predict the behaviour of the material in the area of interest. While this approach might be adequate for an engineer, who only needs a nomogram for numerical purposes, it is not acceptable for someone, who tries to get some differentiated insight into the interdependence of the components making up the system, and their impact on the system behaviour. While these two starting points are only limiting methods, which can hardly be found in practice, a very broad spectrum of methods, which lies in between these two extremes, is in practical use.

1.1 Objective of the work

Having in mind the physics/chemistry in the mesoscopic region, we will restrict ourselves in this work to the tight-binding method. The tight-binding method can be regarded as an adaptation of the well known LCAO method

from theoretical molecular chemistry to solid state problems. The strength of the method rests upon the fact that one is able to handle numerically very large clusters consisting of a variety of elements without the help of symmetry arguments. This is especially important for systems which exhibit no long range ordering. The disadvantage of the method is that one needs a lot of parameters to describe the individual elements in a way which lead to results comparable in quality to the more exact methods such as density functional, pseudopotential or augmented plane wave methods, to mention a few. Normally the parameters are fitted to results obtained with these more 'exact' methods, which in contrast are only applicable to simple ordered structures or very small clusters, due to the limitations of present day computers.

As a guiding principle for our work, we will think of an experimentalist, who wants to do quantum mechanical computations on his/her[1] own for his device/substance. To set the point, we wish to develop a program with the following features:

1. The theoretical basis of the program has to be commonly accepted, and the results should be easy to interpret in terms of common chemical/physical models.

2. The program has to be of great flexibility, to cover a wide range of possible questions.

3. For the input data, we have to look for the practical availability and quality of data.

4. With respect to useability, the program has to fulfill the following prerequisites:

[1]The use of the masculine form is by no means meant discriminatory but follows only the standard language convention.

(a) A user interface which is menu driven and easy to use. Thus it must have a graphical interface.

(b) It should be possible to perform the calculations in reasonable time, i.e. in a range of minutes to a few hours, on a modern PC/workstation, which should be standard in a well equipped laboratory. This means that we wish to be independent of super-computing resources.

Although this is an ambitious programme, we will see that the breathtaking advances in computer hardware, software development tools, and last but not least mathematical progress, have made it possible to get on with this task.

Chapter 2

The tight-binding method

To start with, a short outline of the tight-binding method is given. A good description of the formalism is presented in [79], [65], [29], [84], [64], [33] [26]. As stated in the introduction, the method can be regarded as the solid state adaption of the well known LCAO-method from chemistry [51]. In the tight-binding method the one-electron wave function is expressed as a linear combination of Bloch sums built up from hydrogen like atomic orbitals:

$$\mid \phi^i_{nlm}(\vec{k},\vec{r})\rangle = \frac{1}{\sqrt{N}} \sum_{\vec{R}_n} e^{i\vec{k}(\vec{R}_n+\vec{\rho}_i)} \varphi^i_{nlm}(\vec{r}-\vec{\rho}_i-\vec{R}_n). \tag{2.1}$$

The sum extends over the atoms of the lattice. The function $\varphi^i_{nlm}(\vec{r})$ is the i-th hydrogen like function in the unit cell located at position $\vec{\rho}_i$. The energies for the quantum mechanical eigenvalue problem are found by solving the secular equation

$$\det(\langle \phi_i \mid H - ES \mid \phi_j \rangle) = 0. \tag{2.2}$$

To reduce the computational effort as much as possible, we assume that the atomic functions are orthonormal (this could be achieved by Löwdin orthonormalization, which is preserving the symmetry of the orbitals [43],

[44]). The remaining matrix elements of the Hamiltonian are of the form:

$$E_{ij} = \sum_{\vec{R}_n} e^{i\vec{k}((\vec{R}_m+\vec{\rho}_j)-(\vec{R}_n+\vec{\rho}_i))} \int dv\, \varphi^{i*}_{nlm}(\vec{r}-\vec{\rho}_i-\vec{R}_n) H \varphi^{j}_{nlm}(\vec{r}-\vec{\rho}_j-\vec{R}_m). \tag{2.3}$$

To simplify 2.3 further, we neglect all the three-center integrals and retain only the two center integrals for which we obtain a functional form depending on the connection vector

$$\vec{r} = d \begin{pmatrix} l \\ m \\ n \end{pmatrix}, \quad \| \begin{pmatrix} l \\ m \\ n \end{pmatrix} \| = 1, \quad d = \text{ distance},$$

between the two atoms on which the orbitals are located and their symmetry. E.g., the expression for the matrix element between a p_x- and a $d_{x^2-y^2}$-orbital is:

$$E_{x,x^2-y^2} = \frac{1}{2}\sqrt{3} l(l^2-m^2) V_{pd\sigma} + l(1-l^2+m^2) V_{pd\pi}. \tag{2.4}$$

The complete set of two-center integrals for all hydrogen like functions (in the sense of symmetry) is:

symmetry	two-center expressions
$E_{s,s}$	$V_{ss\sigma}$
$E_{s,x}$	$lV_{sp\sigma}$
$E_{x,x}$	$l^2V_{pp\sigma} + (1-l^2)V_{pp\pi}$
$E_{x,y}$	$lmV_{pp\sigma} - lmV_{pp\pi}$
$E_{x,z}$	$lnV_{pp\sigma} - lnV_{pp\pi}$
$E_{s,xy}$	$\sqrt{3}lmV_{sd\sigma}$
E_{s,x^2-y^2}	$\frac{1}{2}\sqrt{3}(l^2-m^2)V_{sd\sigma}$
$E_{s,3z^2-r^2}$	$[n^2 - \frac{1}{2}(l^2+m^2)]V_{sd\sigma}$
$E_{x,xy}$	$\sqrt{3}l^2mV_{pd\sigma} + m(1-2l^2)V_{pd\pi}$
$E_{x,yz}$	$\sqrt{3}lmnV_{pd\sigma} - 2lmnV_{pd\pi}$
$E_{x,zx}$	$\sqrt{3}l^2nV_{pd\sigma} + n(1-2l^2)V_{pd\pi}$
E_{x,x^2-y^2}	$\frac{1}{2}\sqrt{3}l(l^2-m^2)V_{pd\sigma} + l(1-l^2+m^2)V_{pd\pi}$
E_{y,x^2-y^2}	$\frac{1}{2}\sqrt{3}m(l^2-m^2)V_{pd\sigma} - m(1+l^2-m^2)V_{pd\pi}$
E_{z,x^2-y^2}	$\frac{1}{2}\sqrt{3}n(l^2-m^2)V_{pd\sigma} - n(l^2-m^2)V_{pd\pi}$
$E_{x,3xz2-r^2}$	$l[n^2 - \frac{1}{2}(l^2+m^2)]V_{pd\sigma} - \sqrt{3}ln^2V_{pd\pi}$
$E_{y,3z^2-r^2}$	$m[n^2 - \frac{1}{2}(l^2+m^2)]V_{pd\sigma} - \sqrt{3}mn^2V_{pd\pi}$
$E_{z,3z^2-r^2}$	$n[n^2 - \frac{1}{2}(l^2+m^2)]V_{pd\sigma} + \sqrt{3}n(l^2+m^2)V_{pd\pi}$
$E_{xy,xy}$	$3l^2m^2V_{dd\sigma} + (l^2+m^2-4l^2m^2)V_{dd\pi} + (n^2+l^2m^2)V_{dd\delta}$
$E_{xy,yz}$	$3lm^2nV_{dd\sigma} + ln(1-4m^2)V_{dd\pi} + ln(m^2-1)V_{dd\delta}$
$E_{xy,zx}$	$3l^2mnV_{dd\sigma} + mn(1-4l^2)V_{dd\pi} + mn(l^2-1)V_{dd\delta}$
E_{xy,x^2-y^2}	$\frac{3}{2}lm(l^2-m^2)V_{dd\sigma} + 2lm(m^2-l^2)V_{dd\pi} + \frac{1}{2}lm(l^2-m^2)V_{dd\delta}$
E_{yz,x^2-y^2}	$\frac{3}{2}mn(l^2-m^2)V_{dd\sigma} - mn[1+2(l^2-m^2)]V_{dd\pi} + mn[1+\frac{1}{2}(l^2-m^2)]V_{dd\delta}$
E_{zx,x^2-y^2}	$\frac{3}{2}nl(l^2-m^2)V_{dd\sigma} + nl[1-2(l^2-m^2)]V_{dd\pi} - nl[1-\frac{1}{2}(l^2-m^2)]V_{dd\delta}$
$E_{xy,3z^2-r^2}$	$\sqrt{3}lm[n^2 - \frac{1}{2}(l^2+m^2)]V_{dd\sigma} - \sqrt{3}2lmn^2V_{dd\pi} + \frac{1}{2}\sqrt{3}lm(1+n^2)V_{dd\delta}$
$E_{yz,3z^2-r^2}$	$\sqrt{3}mn[n^2 - \frac{1}{2}(l^2+m^2)]V_{dd\sigma} + \sqrt{3}mn(l^2+m^2-n^2)V_{dd\pi} - \frac{1}{2}\sqrt{3}mn(l^2+m^2)V_{dd\delta}$
$E_{zx,3z^2-r^2}$	$\sqrt{3}ln[n^2 - \frac{1}{2}(l^2+m^2)]V_{dd\sigma} + \sqrt{3}ln(l^2+m^2-n^2)V_{dd\pi} - \frac{1}{2}\sqrt{3}ln(l^2+m^2)V_{dd\delta}$
$E_{x^2-y^2,x^2-y^2}$	$\frac{3}{4}(l^2-m^2)^2V_{dd\sigma} + [l^2+m^2-(l^2-m^2)^2]V_{dd\pi} + [n^2+\frac{1}{4}(l^2-m^2)^2]V_{dd\delta}$
$E_{x^2-x^2,3z^2-r^2}$	$\frac{1}{2}\sqrt{3}(l^2-m^2)[n^2 - \frac{1}{2}(l^2+m^2)]V_{dd\sigma} + \sqrt{3}n^2(m^2-l^2)V_{dd\pi} + \frac{1}{4}\sqrt{3}(1+n^2)(l^2-m^2)V_{dd\delta}$
$E_{3z^2-r^2,3z^2-r^2}$	$[n^2 - \frac{1}{2}(l^2+m^2)]^2V_{dd\sigma} + 3n^2(l^2+m^2)V_{dd\pi} + \frac{3}{4}(l^2+m^2)^2V_{dd\delta}$

The remaining task is to find the V-parameters for the two-center integrals. This could be done in two ways. The first way is, to fit the parameters to experimental data or to more exact calculations at some high symmetry points in the Brillouin zone. This is obviously a method which is only valid for a single given substance. If one is interested in universal properties of condensed matter, it would be preferable to have universal expressions for the V-parameters at hand. A compilation for the periodic table of elements has been given, e.g., by Harrison [29].

$V_{ll'm} = \eta_{ll'm}\frac{\hbar^2}{m_e d^2}$	$V_{ldm} = \eta_{ldm}\frac{\hbar^2 r_d^{3/2}}{m_e d^{7/2}}$	$V_{ddπ} = \eta_{ddm}\frac{\hbar^2 r_d^3}{m_e d^5}$
$\eta_{ssσ} = -1.40$	$\eta_{sdσ} = -3.16$	$\eta_{ddσ} = -16.2$
$\eta_{spσ} = 1.84$	$\eta_{pdσ} = -2.95$	$\eta_{ddπ} = 8.75$
$\eta_{ppσ} = 3.24$	$\eta_{pdπ} = 1.36$	$\eta_{ddδ} = 0$
$\eta_{ppπ} = -0.81$		

Where d is the atomic distance, m_e the electron mass, and r_d is an element dependend adjustable constant.

2.1 LCAO band structures

With the help of these tables, we should always be able to compute for an arbitrary crystalline substance the band structure. The only problem is to work out the needed coupling matrices. For the simpler crystal structures this work has been done by several authors. E.g., the tight-binding matrix for crystalline silicon reads [29], [7], [79]:

	s^1	s^2	p_x^1	p_y^1	p_z^1	p_x^2	p_y^2	p_z^2
s^1	ϵ_s^1	$E_{ss}g_0$	0	0	0	$E_{sp}g_1$	$E_{sp}g_2$	$E_{sp}g_3$
s^2	$E_{ss}g_0^*$	ϵ_s^2	$-E_{sp}g_1^*$	$-E_{sp}g_2^*$	$-E_{sp}g_3^*$	0	0	0
p_x^1	0	$-E_{sp}g_1$	ϵ_p^1	0	0	$E_{xx}g_0$	$E_{xy}g_3$	$E_{xy}g_2$
p_y^1	0	$-E_{sp}g_2$	0	ϵ_p^1	0	$E_{xy}g_3$	$E_{xx}g_0$	$E_{xy}g_1$
p_z^1	0	$-E_{sp}g_3$	0	0	ϵ_p^1	$E_{xy}g_2$	$E_{xy}g_1$	$E_{xx}g_0$
p_x^2	$E_{sp}g_1^*$	0	$E_{xx}g_0^*$	$E_{xy}g_3^*$	$E_{xy}g_2^*$	ϵ_p^2	0	0
p_y^2	$E_{sp}g_2^*$	0	$E_{xy}g_3^*$	$E_{xx}g_0^*$	$E_{xy}g_1^*$	0	ϵ_p^2	0
p_z^2	$E_{sp}g_3^*$	0	$E_{xy}g_2^*$	$E_{xy}g_1^*$	$E_{xx}g_0^*$	0	0	ϵ_p^2

The connection vectors and phase factors are (for a cell constant a):

$$\vec{d_1} = [111]\frac{a}{4} \tag{2.5}$$

$$\vec{d_2} = [1\bar{1}\bar{1}]\frac{a}{4} \tag{2.6}$$

$$\vec{d_3} = [\bar{1}1\bar{1}]\frac{a}{4} \tag{2.7}$$

$$\vec{d_4} = [\bar{1}\bar{1}1]\frac{a}{4} \tag{2.8}$$

$$g_0(\vec{k}) = e^{i\vec{k}\vec{d_1}} + e^{i\vec{k}\vec{d_2}} + e^{i\vec{k}\vec{d_3}} + e^{i\vec{k}\vec{d_4}} \tag{2.9}$$

$$g_1(\vec{k}) = e^{i\vec{k}\vec{d_1}} + e^{i\vec{k}\vec{d_2}} - e^{i\vec{k}\vec{d_3}} - e^{i\vec{k}\vec{d_4}} \tag{2.10}$$

$$g_2(\vec{k}) = e^{i\vec{k}\vec{d_1}} - e^{i\vec{k}\vec{d_2}} + e^{i\vec{k}\vec{d_3}} - e^{i\vec{k}\vec{d_4}} \tag{2.11}$$

$$g_3(\vec{k}) = e^{i\vec{k}\vec{d_1}} - e^{i\vec{k}\vec{d_2}} - e^{i\vec{k}\vec{d_3}} + e^{i\vec{k}\vec{d_4}} \tag{2.12}$$

The matrix elements are:

$$E_{ss} = V_{ss\sigma} \tag{2.13}$$

$$E_{sp} = -V_{sp\sigma}/\sqrt{3} \tag{2.14}$$

$$E_{xx} = \frac{1}{3}V_{pp\sigma} + \frac{2}{3}V_{pp\pi} \tag{2.15}$$

$$E_{xy} = \frac{1}{3}V_{pp\sigma} - \frac{1}{3}V_{pp\pi} \tag{2.16}$$

Taking the lattice constant and nearest neighbor distance from [39], we get the following band structure:

cell constant a	5.43 Å
nearest neighbor distance d	2.35 Å
$V_{ss\sigma}$	−1.932 eV
$V_{sp\sigma}$	+2.539 eV
$V_{pp\sigma}$	+4.471 eV
$V_{pp\pi}$	−1.118 eV

Figure 2.1: Band structure of silicon, parameters from Harrison

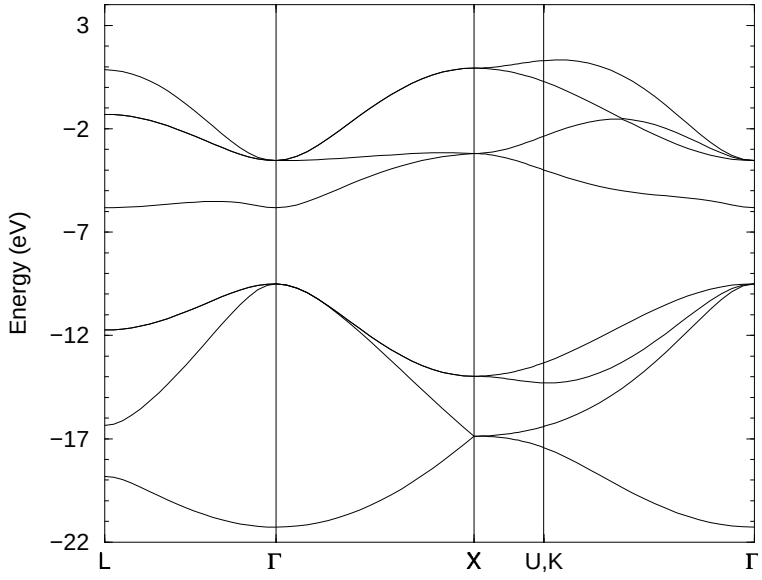

2.2 General approach to LCAO-bands

We should be able by now to compute the band structure for many different elements and compounds. The only time consuming task is to compile the LCAO-matrix, because every different crystal structure needs its own matrix. The dimension of the matrix depends on the number of atoms in the unit cell and the number of orbitals each atom contributes. This is the crucial point for the method. While it is very simple to set up the matrix for a simple compound with only a small number of orbitals, it is quite a different problem to do the same thing for a more complex substance. This can be seen, if one studies the computercodes in the book of Papaconstantopoulos [65]. There we find the listings for many of the most common and simple crystal structures. While the computer code for the simple diamond structure

(eight times eight matrix) runs to four pages, the code for the hexagonal close-packed structure (18 times 18 matrix) runs to 12 pages with hundreds of sine and cosine terms. These terms have been compiled in previous work, mostly on the basis of group symmetry arguments, e.g. [59], [15], [17]. If one is interested in more complex structures, it is evident that this pedestrian approach is no longer feasible. One way to overcome the difficulty is to work out a general computer program, which will construct the LCAO-matrix automatically. This approach is taken here.

2.2.1 A note on software engineering

As stated in the introduction, the objective of the work is the development of a self consistent software tool for large scale quantum mechanical simulations. The approach is a general one, i.e., while writing the program, we have no special substance class in mind, but the whole diversity of possible geometries. This makes the development of the computer code a much more complex task than writing a code for a restricted single purpose. Fortunately, we have today very efficient programming languages and software development environments, which gives us convenient access to the prevalently used program modules, like databases, graphical interfaces, etc. With the help of these languages and tools, we have implemented the following system structure.

The band structure module

Because we want a general program, we can go in principle two ways. One way is to implement for any common structure the band-structure matrix as a separate module. This path was chosen in [65]. The disadvantage of this approach is that every time one is interested in a structure not yet

implemented a new module has to be written. Furthermore, this approach is limited to simple structures, because the band structure matrices for unit cells with more than 18 orbitals are cumbersome or in the end can hardly be handled. As an example, let us think of monoclinic TiO with vacancies. Describing the basic monoclinic unit cell without vacancies (which is by itself a unit cell much harder to investigate than a cubic one) needs 108 orbitals, because the unit cell contains 12 Ti-atoms with five d-orbitals per atom, as well as 12 O-atoms with one s- and three p-orbitals per atom. To print out the resulting matrix needs several meters of paper. The situation becomes even more drastic, if we think of the more complex structures of substances, which are relevant in superconductivity.

The second way is to implement the abstract rules for the matrix set-up, i.e., one implements to a certain extent the rules of group theory which leads to the band-structure matrix. This second approach was taken here. Since the approach is the implementation of our mental manipulations of a crystal, the logical choice for the programming language should be an object orientated one, such as C++. Despite the advantages and the beauty of object orientated languages, the core of the program has been written in Fortran 77/90. The reason is that we end up with a numerical problem, the computation of eigenvalues and eigenvectors, after constructing the matrix. The most efficient routines for numerical purposes are written in Fortran. For comparison and further manipulations some additional routines are written in Mathematica^{TM}. For the database connection, the graphical output, etc. a mixed language mode was chosen, i.e., the combination of C++ and Fortran. To visualize the structure and symmetry operations, we make use of VRML [1], [31]. This new internet language is primarily intended to design interactive 3-dim virtual worlds for games and business purposes. But of course, we

can also use its strength to visualize chemical structures and symmetry operations. It is furthermore possible to get the output in a standard chemical format, like MXYZ, to have access to chemical visualization programs.

The band structure program module requires as input the primitive translation vectors for the Bravais lattice, and the description of the basis in terms of the translation vectors, and the standard symmetry notation for the orbitals; for examples see below. Furthermore the numerical values for the different coupling parameters can be given explicitly, or they are taken automatically from Harrison's solid state table. To compute the band structure, the path in the Brillouin zone is required. From this information the program creates the LCAO-matrix (both numerically as well as symbolically) and computes the band structure of the substance.

As an example, the input files for the simple silicon example reads:

Table 2.1: The input file for the silicon basis

```
* This file contains the basis for Si
* Ref.: Kittel p.29
2
1 Si 0.000 0.000 0.000 4 3S0 3X0 3Y0 3Z0 --- --- --- --- ---
2 Si 0.250 0.250 0.250 4 3S0 3X0 3Y0 3Z0 --- --- --- --- ---
```

Stars serve to denote comments. The first number in the first line is the number of atoms in the unit cell. In the following lines for each atom the number of this atom is given and then the type of atom is labeled in chemical notation (one needs always two letters to label an atom, so oxygen is labeled as Ox and not as O), its position in terms of the lattice vectors, the number of orbitals, and the symmetry label for the orbitals.

Table 2.2: The file for the path in the Brillouin zone

*This is the path in the Brilliouin zone for Silicon which is used by
*Harrison
8.000
20.000
*
0.579–> 0.000
-0.579–> 0.000
0.579–> 0.000
*
0.000–> 0.000
0.000–> 0.000
0.000–> 1.157
*
0.000–> 0.289
0.000–> -0.289
1.157–> 1.157
*
0.000–> 0.000
-0.868–> 0.000
0.868–> 0.000

The first two numbers indicate the number of corner points in the Brillouin zone, respectively the number of points for every edge on which the eigenvalues are computed. Then the corner points are listed. To visualize the whole data set, one can get a graphical output for the Brillouin zone.

The visualization is done with the program MOIL-View written by Carlos Simmerling [78].

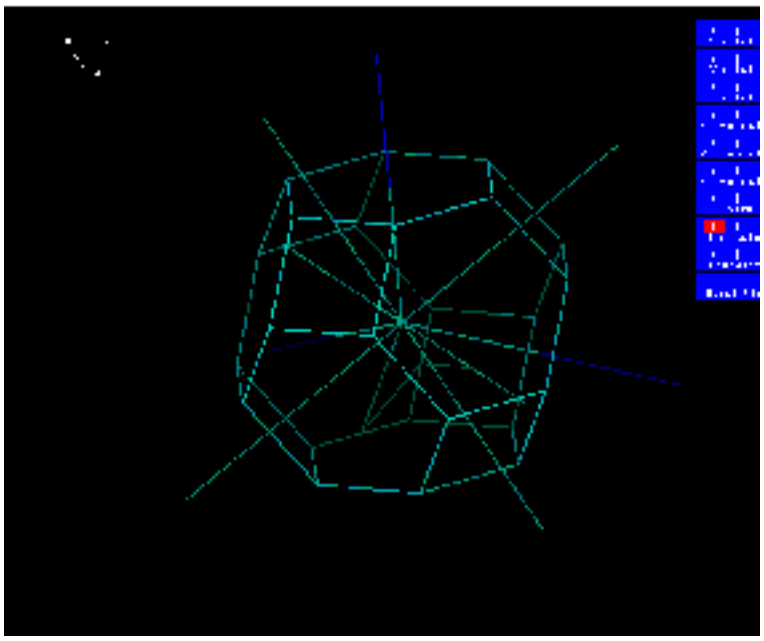

Furthermore, the program needs as input the coupling radius. The coupling radius determines the range for the neighbors (first, second, etc.)

The DOS cluster module

Because we are mainly interested in systems which exhibit no long range ordering, we very often have to compute the spectrum of very large sparse matrices. It is one aim of numerical mathematics to do such computations. For a full diagonalization classical methods scale with N^3. It would be a great advantage to have methods at hand which scale lineary with N. Recently there have been proposals for such methods. Implemented in the software is the method of [76], [77]. The basis forms a maximum entropy method. Its

computational kernel is a matrix vector multiplication, which is well suited for a parallel computer.

2.3 The density of states

Having developed the general tool to compute the band structure of an arbitrary substance, it is no problem to get the second important information for a crystal. This is the density of states (DOS). The DOS can be easily computed by random sampling of the corresponding unit cell of the reciprocal lattice. The parallelepiped of the reciprocal lattice in $\vec{k}-$space is spanned by the reciprocal vectors, which are:

$$\vec{k_1} = 2\pi \frac{\vec{t_2} \times \vec{t_3}}{\vec{t_1} \cdot \vec{t_2} \times \vec{t_3}} \tag{2.17}$$

$$\vec{k_2} = 2\pi \frac{\vec{t_3} \times \vec{t_1}}{\vec{t_1} \cdot \vec{t_2} \times \vec{t_3}} \tag{2.18}$$

$$\vec{k_3} = 2\pi \frac{\vec{t_1} \times \vec{t_2}}{\vec{t_1} \cdot \vec{t_2} \times \vec{t_3}} \tag{2.19}$$

We get the following DOS for silicon (where we have used the parameters of Harrison, 100000 sampling points, and a bin width of 0.1 eV to plot the DOS):

Figure 2.2: DOS of silicon, parameters from Harrison

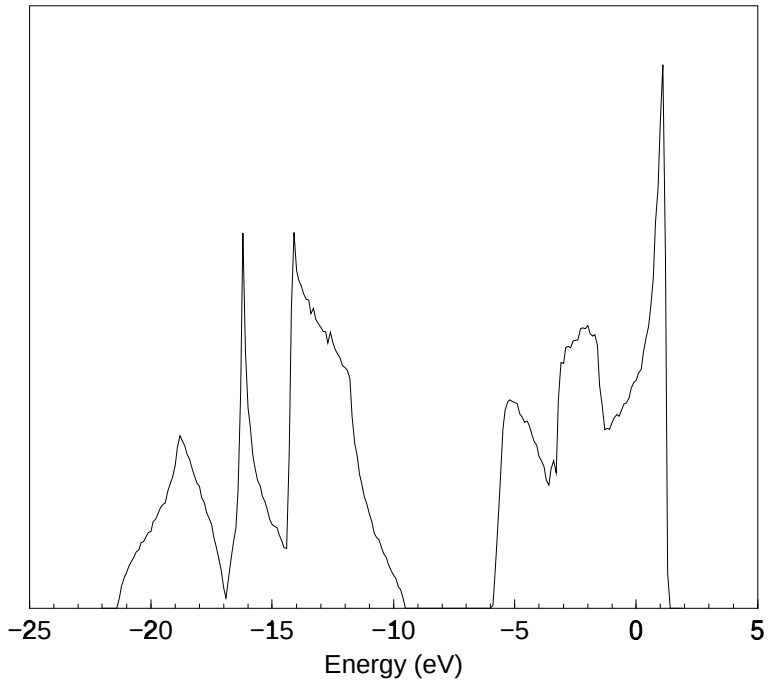

With these two methods and the general code at hand, we are in principle able to compute the more interesting electronic features of a crystalline solid. But as we will see, this is, unfortunately, not quite the reality. The restriction lies in the range of applicability of the parameters listed in the **Solid State Table** of Harrison.

2.4 Some illustrative examples

In the following we will compute some illustrative examples using the Harrison approach, to get a feeling for the range of applicability and the restrictions.

Textbook examples

First we consider the simple s-band models in one, two, and three dimensions [84]. The parameters are:

parameter	value
on-site energy α	-1.0 eV
coupling energy β	-0.1 eV
sampling points	100000
bin width	0.01 eV

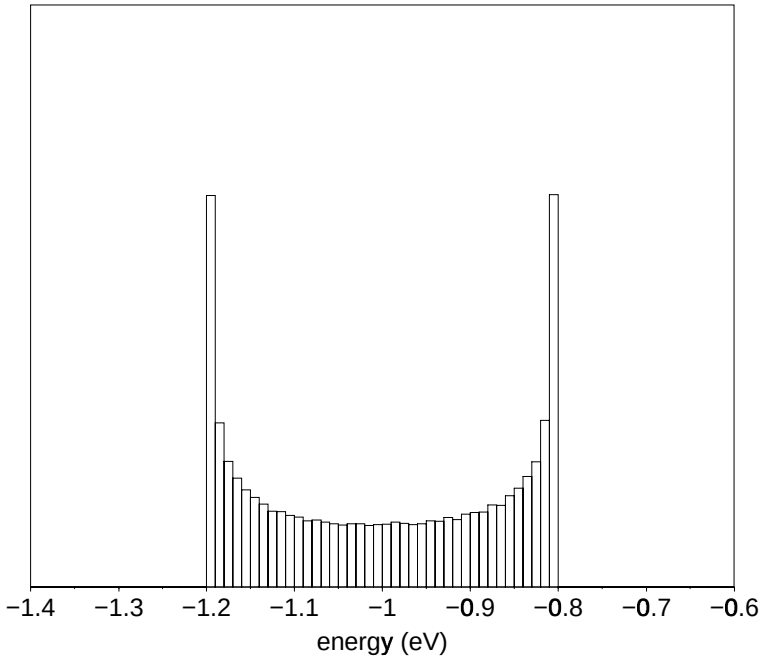

Figure 2.3: DOS of the 1-dimensional s-band model

We get the typical shape for the 1-dimensional DOS, extending from $\alpha-2\beta$ to $\alpha+2\beta$.

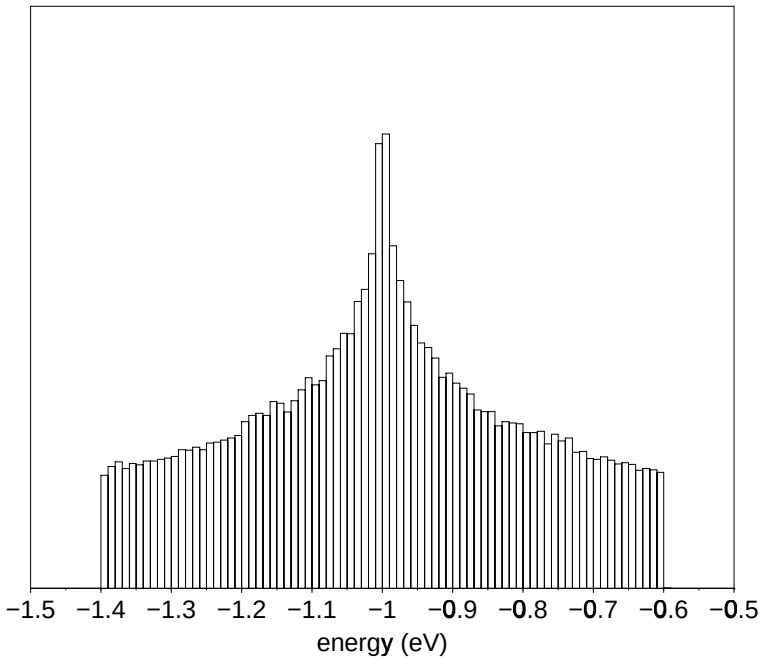

Figure 2.4: DOS for the 2-dimensional s-band model

The DOS extends from $\alpha - 4\beta$ to $\alpha + 4\beta$.

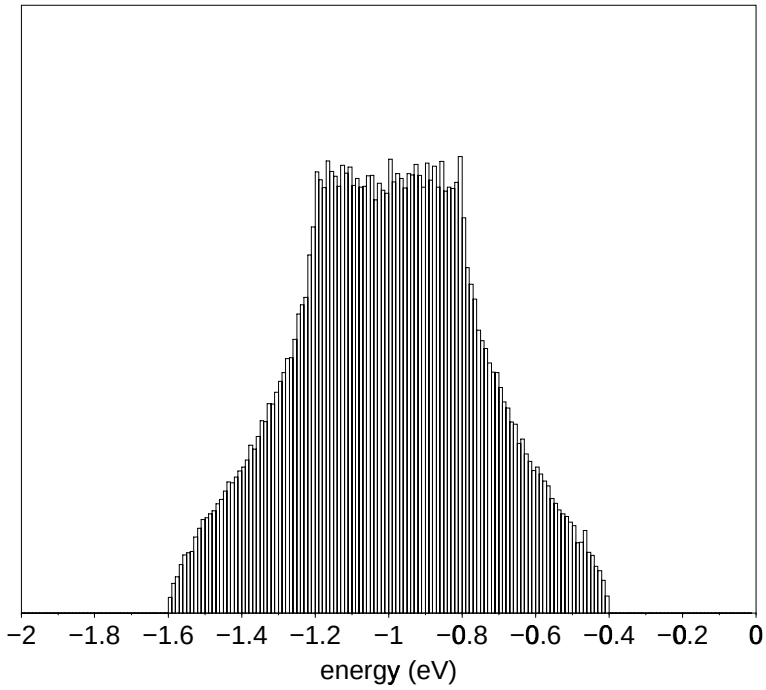

Figure 2.5: DOS for the 3-dimensional s-band model

The DOS extends from $\alpha - 6\beta$ to $\alpha + 6\beta$.

Now we will advance to the more complex examples, to confirm that our program works properly. As a further example we choose the simple cubic tungsten trioxide. The basis consists of one tungsten atom with five 5d-orbitals, and three oxygen atoms with one s- and three p-orbitals each. We treat the full problem, coupling only the first neighbors. The program gets as input:

Table 2.3: The input file for the WO_3 basis

```
* edge length : 3.7845 Angstroem
* ref.: Straumanis, J.Am.Chem.Soc. 71, 679 ('49)
4
1 Wo 0.000 0.000 0.000 5 5X2 5Z2 5XY 5ZX 5YZ ___ ___ ___ ___
2 Ox 0.500 0.000 0.000 4 2S0 2Y0 2Z0 2X0 ___ ___ ___ ___ ___
3 Ox 0.000 0.500 0.000 4 2S0 2X0 2Z0 2Y0 ___ ___ ___ ___ ___
4 Ox 0.000 0.000 0.500 4 2S0 2X0 2Y0 2Z0 ___ ___ ___ ___ ___
```

Table 2.4: The input file for the path in the Brillouin zone

```
* G -> X -> M -> G -> R -> X
10.000
50.000
*
0.000–> 0.831
0.000–> 0.000
0.000–> 0.000
*
0.831–> 0.831
0.000–> 0.000
0.000–> 0.831
*
0.831–> 0.000
0.000–> 0.000
0.831–> 0.000
*
0.000–> 0.831
0.000–> 0.831
0.000–> 0.831
*
0.831–> 0.831
0.831–> 0.000
0.831–> 0.000
```

Table 2.5: The parameters for WO_3 from Harrison

cell constant a	3.7845 Å
first neighbor distance d	1.9 Å
on-site oxygen s	−29.14 eV
on-site oxygen p	−14.13 eV
on-site tungsten d	−10.96 eV
$V_{sd\sigma}$	−3.6976 eV
$V_{pd\sigma}$	−3.4519 eV
$V_{pd\pi}$	+1.5914 eV

Figure 2.6: Band structure of WO_3, parameters from Harrison

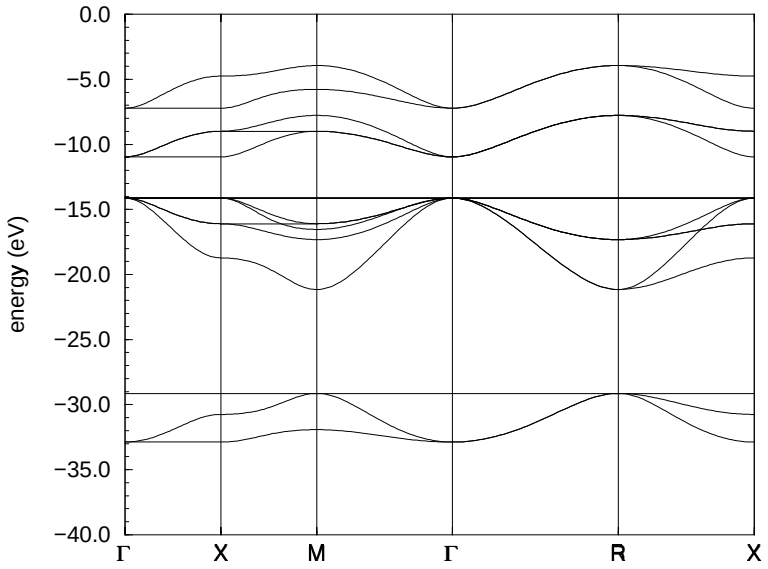

The bands are in agreement with the computations done by Wolfram [89], Mattheiss [45], and Dücker [14], and for analogous structures [8], [40], [81]. By sampling the Brillioun zone, we get the DOS.

parameters	Harrison
coupling	first nearest neighbors
sampling points	10000
bin width	0.1 eV

Figure 2.7: DOS of WO_3, parameters from Harrison

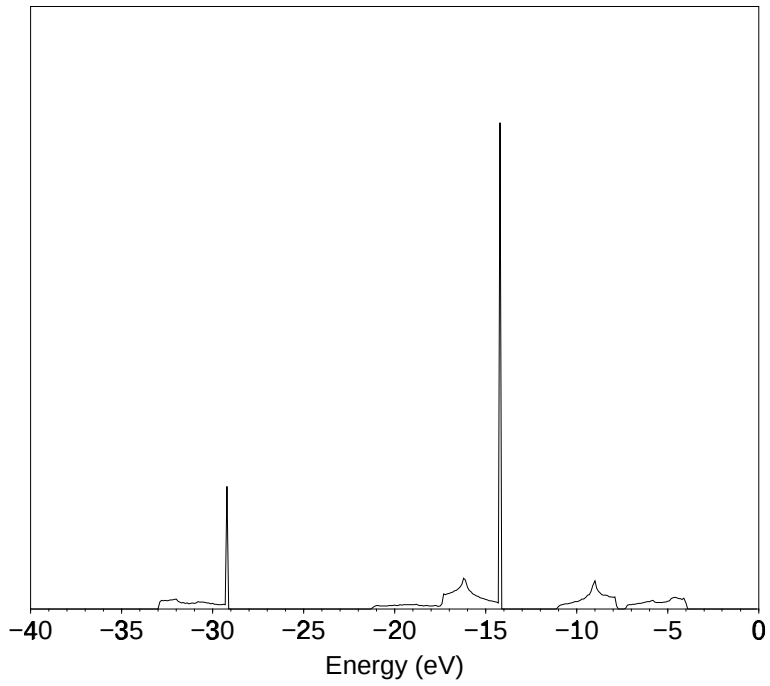

Because of the two dispersionless bands, we have two pronounced peaks. To give these two bands a dispersion, one must widen the coupling range.

2.5 The breakdown of the method

Having found that all the examples, given in Harrison's book so far, are correctly reproduced, we are convinced that every arbitrary substance should

be computable. As a next example we choose a more complex substance, RuO_2. The Bravais lattice is tetragonal, and the translation vectors are:

$$\vec{t_1} = a\vec{i}, \qquad \vec{t_2} = a\vec{j}, \qquad \vec{t_1} = c\vec{k},$$

where a and c are the lattice parameters. The basis reads in terms of these vectors:

Table 2.6: The input file for the RuO_2 basis

```
* ref.: Mattheiss, Phys. Rev. B, 13, No.6, pp. 2433 - 2450, (1976)
6
1 Ru 0.000 0.000 0.000 5 3Z2 3X2 3XY 3ZX 3YZ ___ ___ ___ ___
2 Ru 0.500 0.500 0.500 5 3Z2 3X2 3XY 3ZX 3YZ ___ ___ ___ ___
3 Ox 0.306 -0.306 0.000 4 2S0 2Y0 2Z0 2X0 ___ ___ ___ ___ ___
4 Ox -0.306 0.306 0.000 4 2S0 2Y0 2Z0 2X0 ___ ___ ___ ___ ___
5 Ox 0.194 0.194 0.500 4 2S0 2Y0 2Z0 2X0 ___ ___ ___ ___ ___
6 Ox -0.194 -0.194 -0.500 4 2S0 2Y0 2Z0 2X0 ___ ___ ___ ___ ___
```

The unit cell is given in the following figure:

Figure 2.8: Unit cell of RuO_2

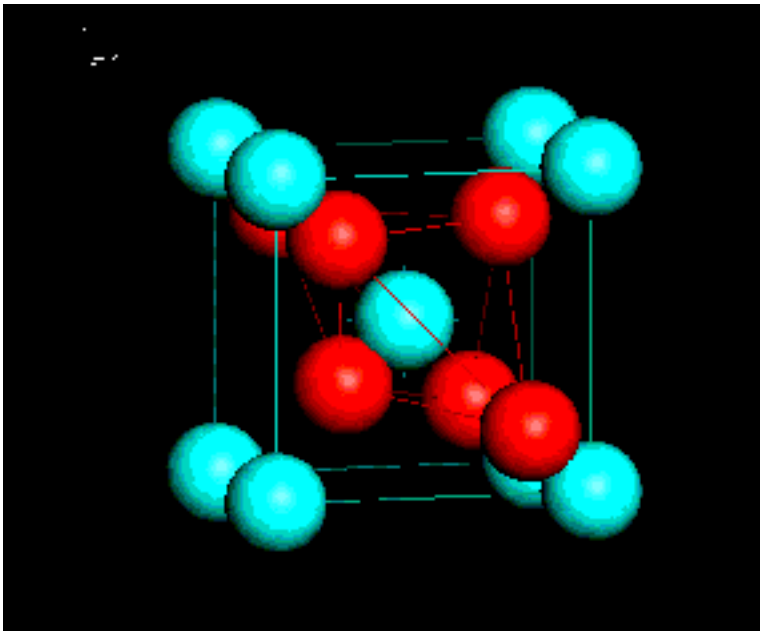

The space group for the rutile structure is $D_{4h}^{14}(P4_2/mnm)$ which is non-symmorphic. The low symmetry of the structure makes it difficult to work out the corresponding tight-binding matrix, as Mattheiss wrote citeMattheiss3. The needed group theoretical work is presented in [15] and [61]. To compare the results with the work of Mattheiss [47], we take his coupling structure:

Table 2.7: Coupling structure for RuO_2, Mattheiss [47]

edge length	a	4.4919 Å
edge length	c	3.1066 Å
position	u	0.306
parameters		
A-A	$d_1 = c$	3.107 Å
	$d_2 = [\frac{1}{2} + (c/2a)^2]^{\frac{1}{2}}a$	3.536 Å
	$d_3 = a$	4.492 Å
A-B	$d_1 = \sqrt{2}ua$	1.944 Å
	$d_2 = [2(\frac{1}{2} - u)^2 + (c/2a)^2]^{\frac{1}{2}}a$	1.983 Å
B-B	$d_1 = \sqrt{2}(1 - 2u)a$	2.465 Å
	$d_2 = [\frac{1}{4} + (\frac{1}{2} - 2u)^2 + (c/2a)^2]^{\frac{1}{2}}a$	2.777 Å
	$d_3 = c$	3.107 Å
	$d_4 = [(1 - 2u)^2 + (2u)^2]^{\frac{1}{2}}a$	3.255 Å

The resulting DOS is:

Table 2.8: DOS for RuO_2 parameters

parameters	Harrison
coupling	Mattheiss [47]
sampling points	10000
bin width	0.01

Figure 2.9: DOS of RuO_2, parameters from Harrison

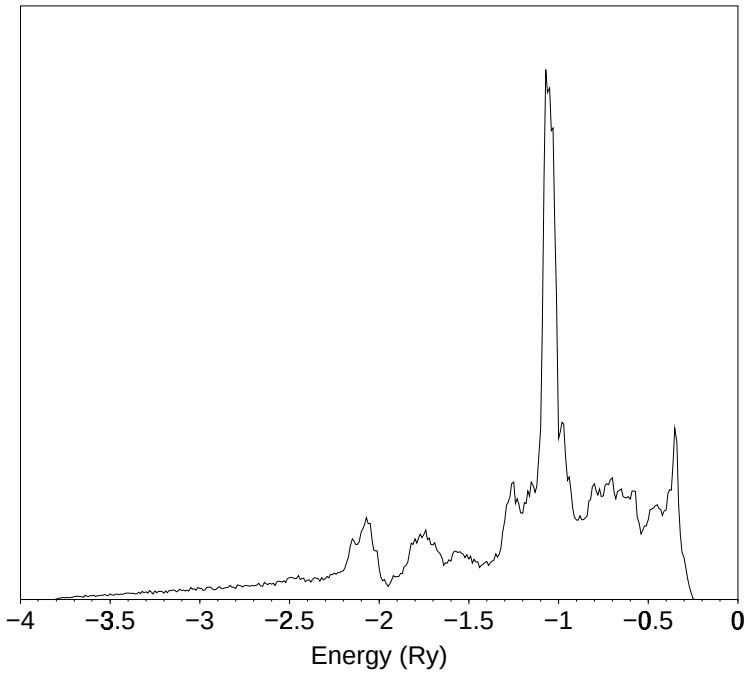

RuO_2 is correctly predicted to be a metal, but the DOS looks by no means similar to the one given by Mattheiss (see below). The reason could be twofold. Either our program has made a mistake in computing the DOS or something is going wrong with the parameters. To study this, we apply the parameters given by Mattheiss. Because Mattheiss is working with a slightly different description for the substance including overlap and different p-orbital energies, we have to adjust his parameters. To be consistent with the prevalent notation in the literature, we abbreviate the V_{abc} notation to $(abc)_n$, where the subscript refers to the distance or the neighbor shell.

Table 2.9: Parameters for RuO_2 given by Mattheiss and the adjusted values

Type	Mattheiss	Adjusted	Type	Mattheiss	Adjusted
E_s	-1.1887		$(dd\sigma)_2$	-0.0095	
$(ss\sigma)_1$	-0.0181		$(dd\pi)_2$	0.0003	
$(ss\sigma)_2$	-0.0083		$(dd\delta)_2$	0.0002	
$(ss\sigma)_3$	-0.0057		$(dd\sigma)_3$	0.0073	
E_{x+y}	-0.0747	-0.0850	$(dd\pi)_3$	0.0018	
E_{x-y}	-0.0980	-0.0850	$(dd\delta)_3$	-0.0028	
E_z	-0.0906	-0.0850	$(sd\sigma)_1$	-0.1633	
$(pp\sigma)_1$	0.0466		$(S_s)_1$	0.0361	0.0000
$(pp\pi)_1$	-0.0161		$(pd\sigma)_1$	-0.1849	
$(pp\sigma)_2$	0.0290		$(S_\sigma)_1$	0.0838	0.0000
$(pp\pi)_2$	-0.0056		$(pd\pi)_1$	0.0816	
$(pp\sigma)_3$	0.0181		$(S_\pi)_1$	-0.0848	0.0000
$(pp\pi)_3$	-0.0001		$(sd\sigma)_2$	-0.1837	
$(pp\sigma)_4$	0.0159		$(S_s)_2$	0.0590	0.0000
$(pp\pi)_4$	-0.0006		$(pd\sigma)_2$	-0.1638	
E_d	0.1591		$(S_\sigma)_2$	0.0748	0.0000
$(dd\sigma)_1$	-0.0366		$(pd\pi)_2$	0.0722	
$(dd\pi)_1$	0.0039		$(S_\pi)_2$	-0.0136	0.0000
$(dd\delta)_1$	0.0019				

With these parameters we are able to reproduce the DOS obtained by Mattheiss:

Figure 2.10: DOS of RuO_2, parameters from Mattheiss (adjusted)

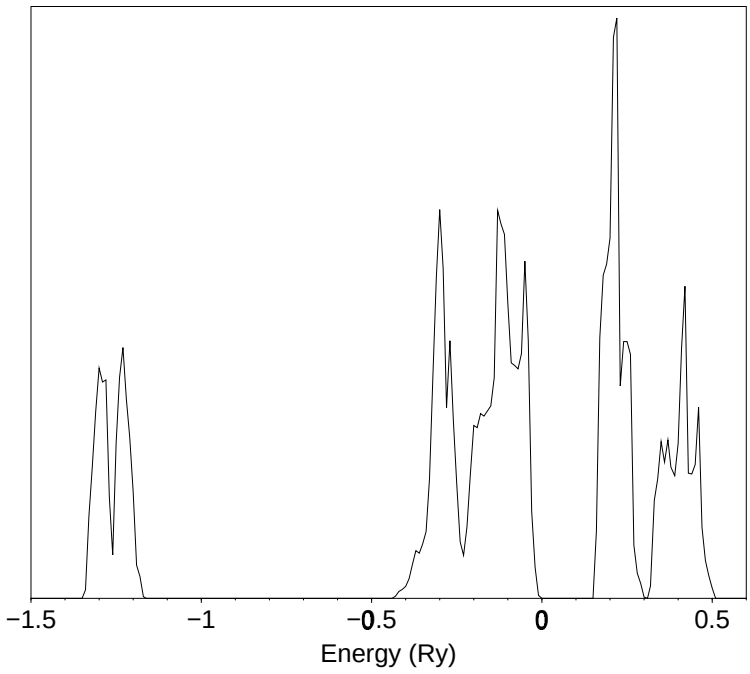

This agreement with the work of Mattheiss proves that the program is working correctly. We have to conclude that the parameters given by Harrison are not valid in general. The rich distance structure of the RuO_2 systems allows for a direct comparison of the parameters given by Harrison and Mattheiss. To this aim we interpolate the Mattheiss parameters with a polynomial fit function and plot the resulting function in comparison with the Harrison scaling law. This is done for all different types of V-parameters.

Figure 2.11: Comparison for $V_{ss\sigma}$

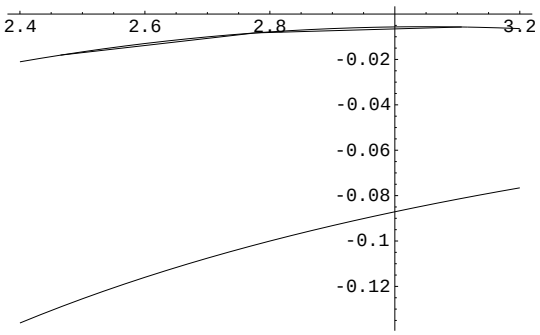

Figure 2.12: Comparison for $V_{pp\sigma}$

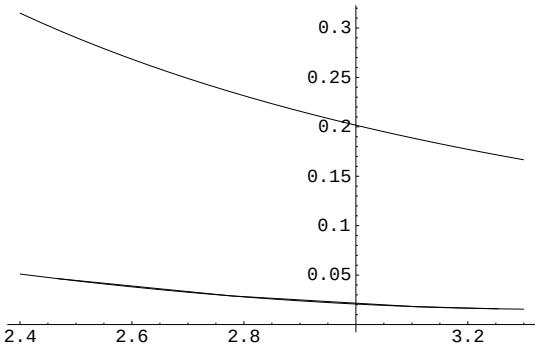

Figure 2.13: Comparison for $V_{pp\pi}$

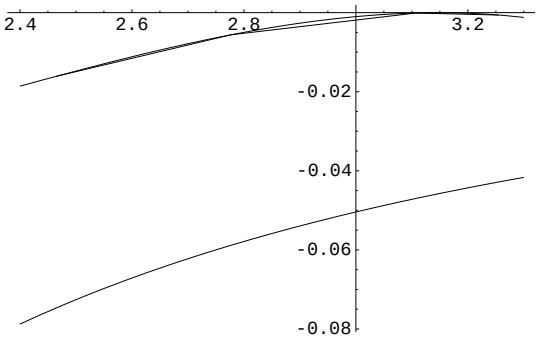

Figure 2.14: Comparison for $V_{dd\sigma}$

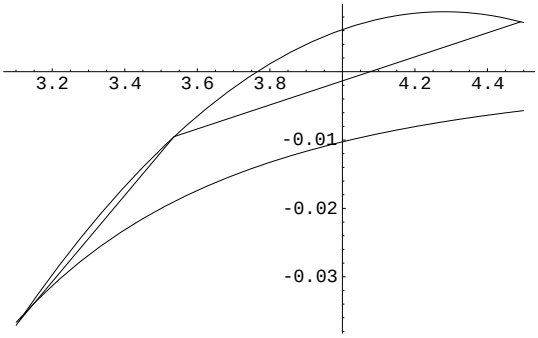

Figure 2.15: Comparison for $V_{dd\pi}$

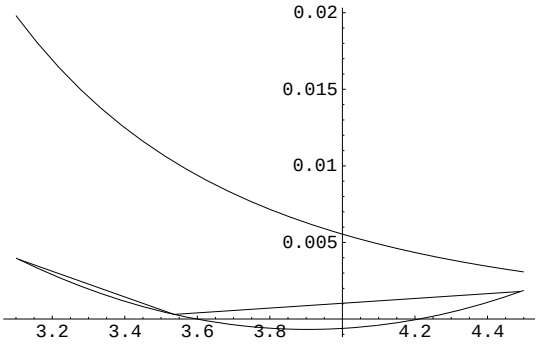

Figure 2.16: Comparison for $V_{dd\delta}$

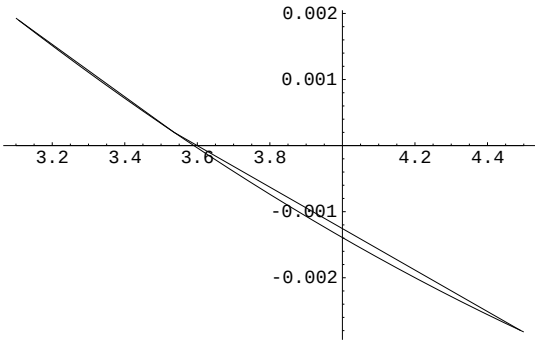

Figure 2.17: Comparison for $V_{sd\sigma}$

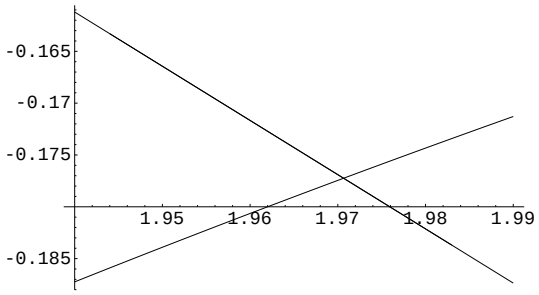

Figure 2.18: Comparison for $V_{pd\sigma}$

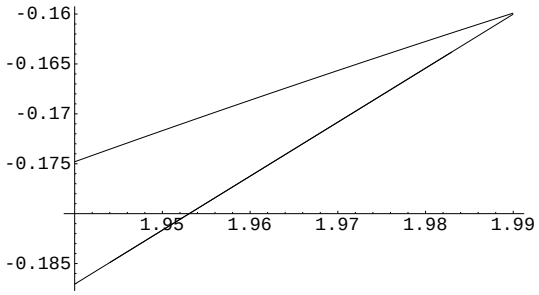

Figure 2.19: Comparison for $V_{pd\pi}$

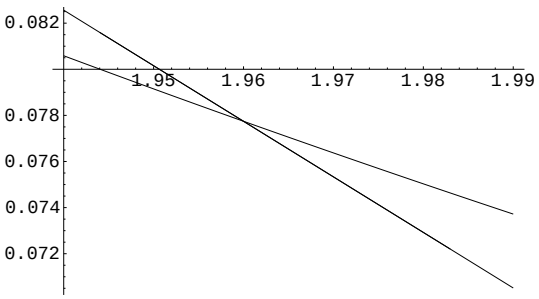

The comparison of our polynomial fit with the scaling laws given by Harrison shows for most of the parameters a great similarity in the curvature. The

main difference is an absolute shift in the curves. Only the parameter $V_{sd\sigma}$ is completely at odds. The two proposed scaling laws show the opposite slope.

It has to be clearly stated that the failure of the general method can be found in the fact that we have used Harrisons parameters for a longer coupling range than only first nearest neighbors. In his book [29], Harrison pointed out that his parameters should only be used for first nearest neighbor coupling. But the restriction to first nearest neighbors makes the tight-binding method too inaccurate in this case. We will see this from the example of TiO_2. This substance has like RuO_2 a rutile structure. For the structural and electronic properties see [88], [62], [6], [60], [23], [11], and [5]. First we compute the DOS with the help of Harrison's solid state table.

Table 2.10: TiO_2 DOS data

parameters	Harrison
coupling	first nearest neighbors
sampling points	10000
bin width	0.1

Figure 2.20: DOS of TiO_2, parameters from Harrison

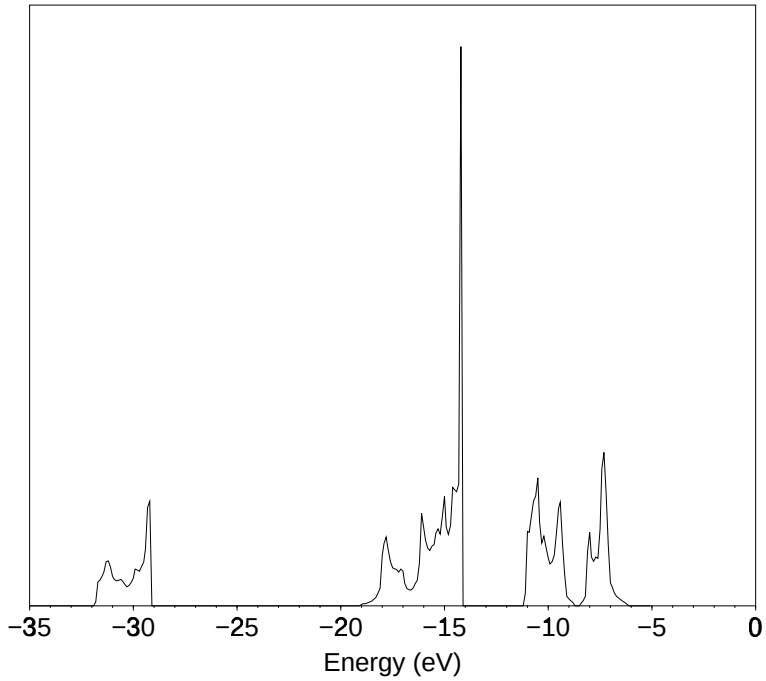

The experimentally observed 2p-3d fundamental energy gap of 3.0 eV is correctly predicted. The large peak at approximately -14 eV stems from a band without dispersion. To give it a dispersion which it ought to have, we have to extend the coupling range. A range of 3.6 Å leads to the following result:

Figure 2.21: DOS of TiO_2, parameters from Harrison, extended coupling range

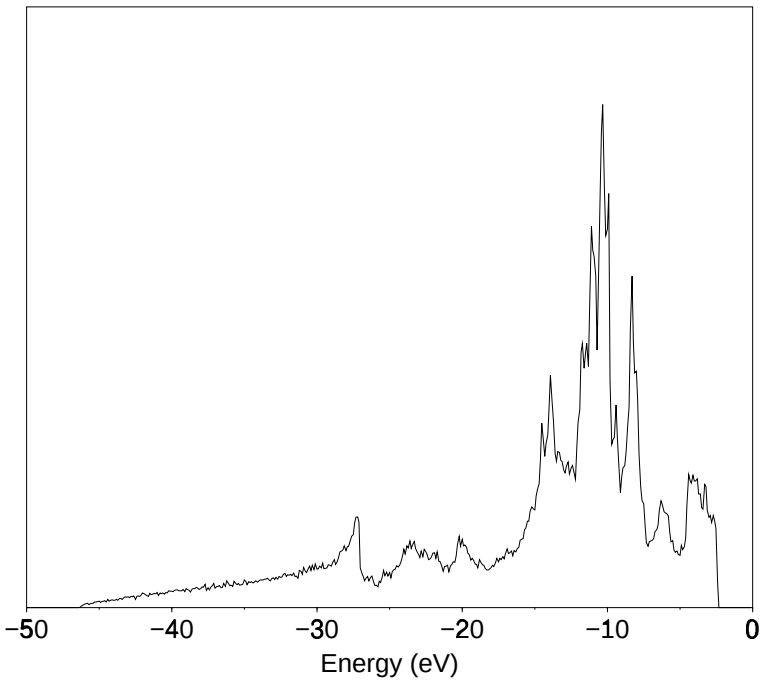

The result is totally inappropriate and meaningless. The important band gap has totally disappeared. Because we investigate the same geometric structure, the resulting DOS resembles the one of RuO_2. And as we have seen there, a special parameter set has to be used. For the TiO_2 example, we choose the parameter set of Vos [88].

Table 2.11: Parameters for TiO_2 from Vos

		d (Å)	E (eV)	d (Å)	E (eV)	d (Å)	E (eV)
Ti	$E_{d\sigma}$	0.0	-6.4				
Ti	$E_{d\pi}$	0.0	-6.4				
O	$E_{p\sigma}$	0.0	-10.5				
O	$E_{p\pi}$	0.0	-10.5				
O	E_s	0.0	-25.0				
Ti-O	$pd\sigma$	1.94	-2.30	1.99	-2.30		
Ti-O	$pd\pi$	1.94	1.15	1.99	1.15		
Ti-O	$sd\sigma$	1.94	-2.50	1.99	-2.50		
O-O	$pp\sigma$	2.52	0.60	2.78	0.40	2.96	0.25
O-O	$pp\pi$	2.52	-0.12	2.78	-0.08	2.96	-0.05
Ti-Ti	$dd\sigma$	2.96	-0.500	3.57	-0.200	4.59	0.0
Ti-Ti	$dd\pi$	2.96	0.260	3.57	0.104	4.59	0.0
Ti-Ti	$dd\delta$	2.96	-0.0350	3.57	-0.014	4.59	0.0

With this parameter set we can perfectly reproduce the band structure given in the work of Vos.

Figure 2.22: Band structure of TiO_2, parameters from Vos

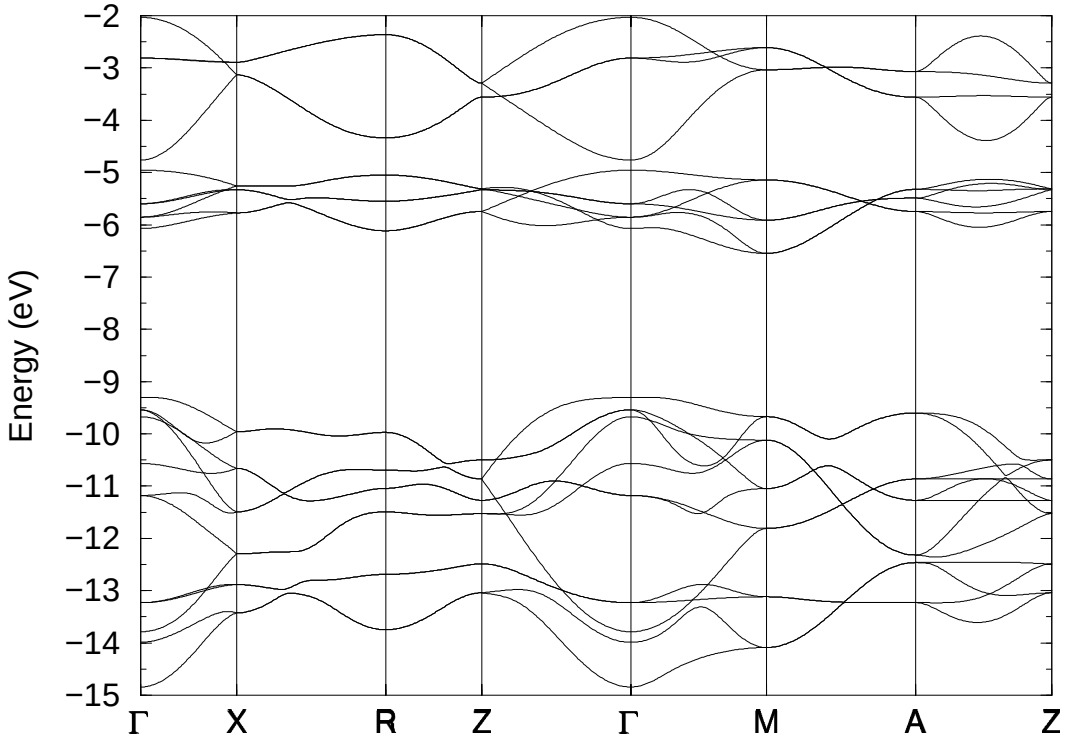

The more reliable DOS, which was computed in [62] is then:

Figure 2.23: DOS of TiO_2, parameters from Vos

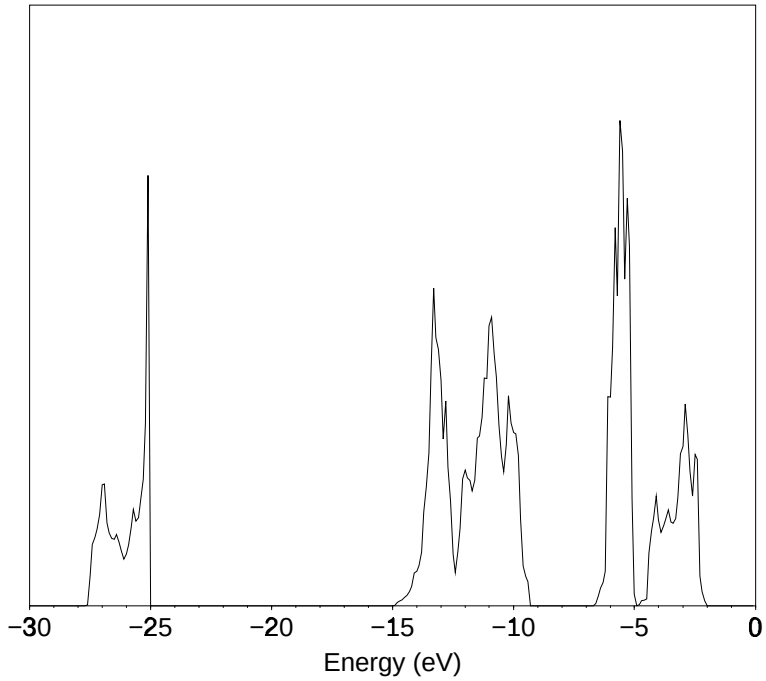

2.6 Conclusion

From the examples above it should be clear that the general LCAO method forms a powerful tool to describe the electronic structure of an arbitrary substance. But as we have seen, the correct choice of the parameters is by no means trivial. A general solid state table gives only a first and quick impression of the substance, but it does not provide high quality results. To get results which are more reliable, one has to work out a special parameter set. This parameter set has to include for the majority of substances at least second nearest neighbor coupling. This requirement is intuitively clear from physical reasons. To recognize this, we go back to the examples with the rutile structure. The band structure is of course dominantly influ-

enced by the octahedron in the center of the unit cell (see figure 2.8). This octahedron is correctly described by the assumption of first nearest neighbor coupling. But clearly the long range ordering of the octahedrons must have also an influence of the electronic structure. To take the long range ordering into account, we have to compute a larger coupling sphere. But for this larger sphere the global Harrison parameters give no longer valid results.

Finally we show the direct comparison of the two densities of states:

Figure 2.24: DOS of TiO_2, parameters from Harrison

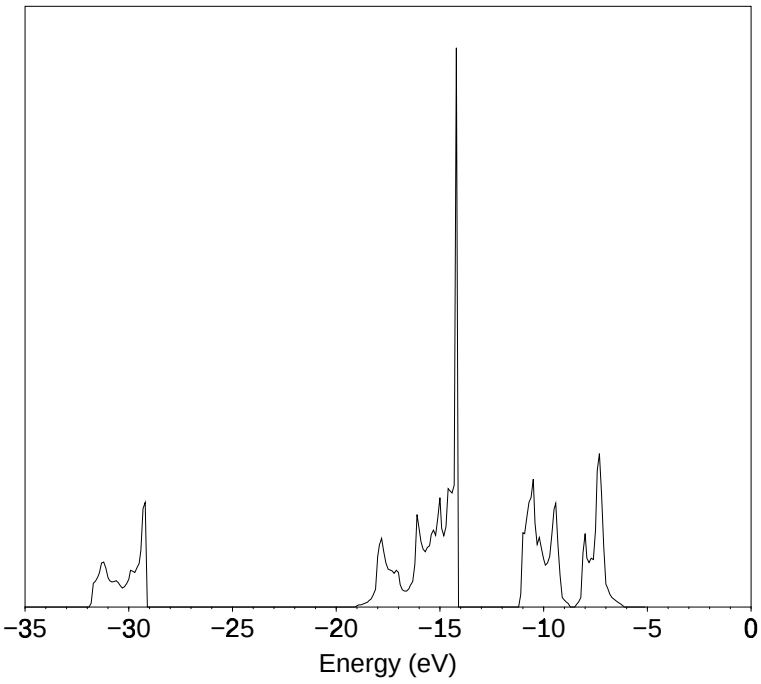

Figure 2.25: DOS of TiO_2, parameters from Vos

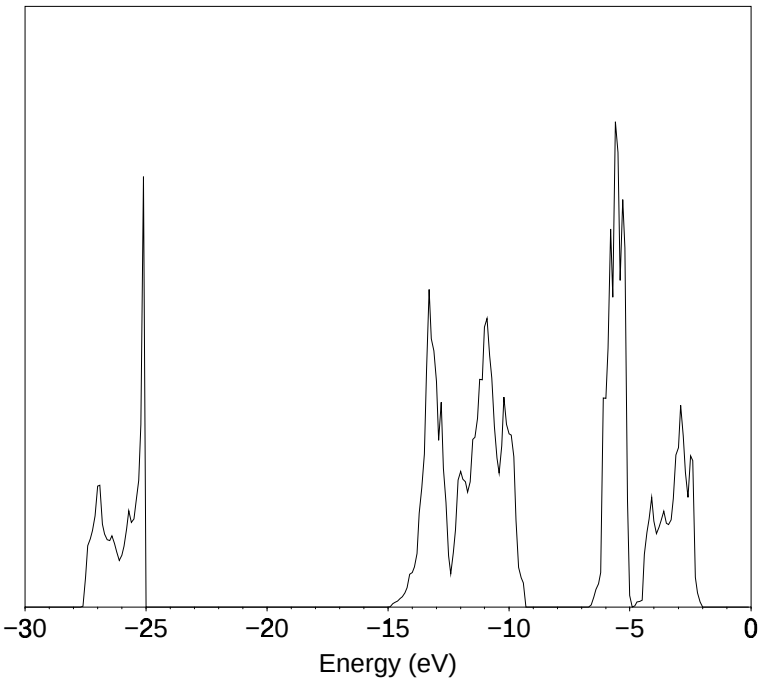

Chapter 3

Fitting a band structure

From the above sections it should be abundantly clear that there is no general set of parameters and scaling laws for describing the whole world of solid state physics and chemistry. It depends on the special system under investigation which parameters have to be chosen. In the following we will develop a general method to find high quality parameters for an arbitrary substance. We further require that the method does not request any special knowledge about the global behaviour of the parameters by the user. This means, we want a fully automated version of a parameter search algorithm.

Looking into the literature, we find that there are mainly two different ways for the parameter fitting. The simplest way is to find the needed parameters by an 'educated guess'. This 'method' requires indeed a very good knowledge of the tight-binding theory and works only in a simple set-up. So the method is restricted to the experienced user. There are many examples in the literature, where one has found the parameters by experience and more or less strong physical reasoning [48], [36], [88]. Without any deeper insight, one could try to find the parameters by trial and error, a very dry and tedious task [82], [88]. It is therefore evident that an automated search algorithm is

of great advantage. To set up such an algorithm, we recast our search problem into an optimization problem. The objective function is an adequately chosen distance between the tight-binding band structure and the objective band structure, which may be computed by a more elaborate method such as augmented plane wave (APW), Korringa, Kohn, and Rostoker (KKR), linear muffin-tin orbital (LMTO), density functional theory (DFT), etc. The remaining fitting task is a nonlinear least-squares fitting problem. The problem is that of adjusting the LCAO parameters to minimize D, the sum of the weighted squares of residuals, where

$$\mathrm{D} = \sqrt{\frac{1}{M}\sum_{\vec{k},n} w_{\vec{k},n}(\mathrm{E}_{\vec{k},n} - \epsilon_{\vec{k},n})^2}, \tag{3.1}$$

and $\mathrm{E}_{\vec{k},n}$ and $\epsilon_{\vec{k},n}$ are the n LCAO and exact energies (in total there are M energy values) at point $\vec{k}$ [46]. In general the $E_{\vec{k},n}$ are nonlinear functions of the parameter vector $\vec{p} = \{\mathrm{p}_1, ..., \mathrm{p}_j\}$. This can be seen as follows [12]. The matrix elements of the Hamiltonian between two Bloch sums depend linearly on the LCAO parameters p_i. The dependence of the energy eigenvalues on p_i is given by the Hellman-Feynman theorem [68]:

$$\frac{\partial E_n^{\mathrm{LCAO}}(\vec{k})}{\partial \mathrm{p}_i} = \vec{c}_n^{\,t}(\vec{k})\frac{\partial H(\vec{k})}{\partial \mathrm{p}_i}\vec{c}_n(\vec{k})$$

This is not a linear dependence because the eigenvectors $\vec{c}_n(\vec{k})$ depend on the parameters p_i as well. If the $E_{\vec{k},n}$ were linear functions of $\vec{p}$, one could numerically solve the set of linear equations which arise from setting

$$\frac{\partial \mathrm{D}}{\partial \mathrm{p}_i} = 0 \text{ for } i \in \{1, ..., j\}. \tag{3.2}$$

In the non-linear case, one has to choose an iterative method, e.g., a Taylor-series expansion method [46], [72]. To improve the convergence behaviour, the method of Hartley [30] proved to be useful, or one could rely on an

implemented standard method, such as the direction set method of Powell [71] or the Levenberg-Marquardt algorithm [71], [53]. Such an algorithm is capable of computing the needed parameters from a properly chosen starting vector $\vec{p}$. The choice of the starting vector remains a nontrivial task, because if the starting vector is not well chosen, the fitting algorithm will get trapped in one of the many local minima, which might be rather useless. But even if we have found the global minimum, we have to be aware of the fact that the parameters, which have been found by the optimization algorithm, are sometimes not physically meaningful. A minimal distance is not equivalent to physically reasonable parameters. As we will see in section 3.1.2, a poorer distance may result in parameters, which better represents the physics. Thus the task we are facing is not a true optimization problem. Many attempts have been made to avoid unphysical parameters. E.g., a symmetrized basis ensures that the LCAO eigenvalues and APW eigenvalues belong to the same irreducible representation [12], [53].

Up to now all the introduced methods have in common that they require a complex manipulation of the LCAO matrix. E.g., the symmetrized basis requires a unitary transformation, which splits the hamiltonian into submatrices belonging to the same various irreducible representations. Furthermore, to find the start vector, the hamiltonian has to be block-diagonalized and approximated at the fit-points, which are selected high symmetry points in the Brillouin zone [65] (see section 3.2.) It should be clear that such a complex manipulation can only be done for relatively simple matrices.

To avoid the manipulation of the LCAO matrix and the knowledge of a good starting point in parameter space, we will go another route. We choose as an optimization algorithm a random search. In the last few years there have been several proposals for such random search algorithms, which

proved to be of great importance. These algorithms belong to the classes of simulated annealing algorithms, evolutionary programming, and genetic algorithms. Especially in engineering problems these algorithms were able to solve even very complex problems which were out of reach for the classic optimization tools. The use of a genetic algorithm for fitting the bands in the class of zinc-blende structures can be found in [83]. Ten populations running on Sun 10-52 workstations provide after ten hours a set of parameters, which is judged by the authors as superior to those achieved by traditional methods. Evolutionary programming algorithms have so far not been applied to the problem at hand.

Another class of algorithms, which has come into vogue, are neural networks, but the attempt to fit the band structure by using feedforward neural networks proved to be very difficult [82].

3.1 Simulated annealing

For our purposes, we introduce a variation of the well known simulated annealing algorithm, called self adapting simulated annealing. This algorithm proves to be very fast and robust. Its simple algorithmic structure makes its implementation easy in terms of the global structure modules. Thus no restriction to a special structure is given and our claim of generality is fulfilled.

Simulated annealing was introduced as a Monte Carlo technique in statistical physics [58]. Since then the method was constantly expanded and applied to many different optimization problems [38], [37]. In the conventional set-up, called Boltzmann annealing, the method works as follows:

1. Given a state $\vec{s}_{\text{old}}$ in a d-dimensional state space, one randomly chooses a new state $\vec{s}_{\text{new}}$ according to a probability law. The increments in the

individual dimensions are independently and normally distributed, so one works with a d-dimensional Gaussian distribution:

$$\mathrm{pdf}_{\vec{s}_{\mathrm{old}}}(\vec{s}_{\mathrm{new}}) = (2\pi T)^{-d/2} \exp[-(\vec{s}_{\mathrm{new}} - \vec{s}_{\mathrm{old}})^2/(2T)] \tag{3.3}$$

The variance T, called the temperature, of this random walk is not constant but depends on a schedule.

2. For the new state the cost function $E(\vec{s})$ is evaluated. If this function decreases, one accepts the new state. In case of an increase the new state is accepted according to an acceptance probability, i.e., one draws a random number from a uniform distribution over $[0, 1]$. If the number is smaller then

$$h_{\vec{s}_{\mathrm{old}}}(\vec{s}_{\mathrm{new}}) = \frac{1}{1 + \exp[(E(\vec{s}_{\mathrm{new}}) - E(\vec{s}_{\mathrm{old}}))/T]}, \tag{3.4}$$

one accepts the new state, in the opposite case one rejects the new state.

3. In the course of the process the temperature is constantly decreased. The art of simulated annealing consists mainly in choosing a good temperature schedule. If one is cooling down the process too quickly, it will get captured in a local minimum. If the process is cooled too slowly, the computing time will be excessive. Given $\mathrm{pdf}_{\vec{s}_{\mathrm{old}}}(\vec{s}_{\mathrm{new}})$, it has been proven [22] that it should be sufficient to cool down not faster than

$$T(k) = \frac{T_0}{\ln(k)} \tag{3.5}$$

to reach the global minimum, where k is the step index.

While the above set-up is based on a strong physical analogy/reasoning (the annealing of a physical system, which is falling into an energetic minimum),

it is by no means mandatory. Being aware of the fact that we only need a heuristic approach, we can widely vary the three introduced functionals. This has led in the past to many different approaches. To mention a few, these are fast annealing [86], very fast annealing, very fast simulated reannealing [34], [35].

3.1.1 Self adapting simulated annealing

We are by no means the first who try to solve the optimization problem with the help of a simulating annealing algorithm. The method itself was successfully applied by many authors, see e.g. [41], [16], [3]. One disadvantage of the random search methods is that their great flexibility with respect to the starting point in parameter space must be compensated by more computing time. A typical optimization run may cost several hours or even one or two days [41], [83]. In the present work we wish to introduce a different heuristic approach for searching which turns out to be very fast. The intention of the algorithm is to search the parameter space on different length scales in a decreasing order. The algorithm works as follows:

1. For tight-binding theory all parameters are expressed as $a.bcde$ with four figures beyond the decimal point.

2. First we determine the sign of the parameters (see chapter 4). Having chosen the sign, we choose $+1.0000$ as starting value for the parameters with a positive sign, and -1.0000 for those with a negative sign.

3. The algorithm starts to change randomly and independently every parameter one digit at position b maximally by one unit, i.e., we draw a random number from a uniform distribution over $[-0.1, 0.1]$ and add it

to b. It presents no problems if the order of magnitude of a parameter is different from the starting value.

4. In an initialization phase, the algorithm computes the mean change in the objective function in case of a deterioration in the cost function $\langle E(\vec{s}_{\text{new}})^{\text{ deterioration}} - E(\vec{s}_{\text{old}})\rangle$.

5. In case of a decrease in the objective function, the new state is accepted, in case of an increase, the new state is accepted if a uniformly distributed random number over $[0, 1]$ is less than

$$\exp(-\frac{E(\vec{s}_{\text{new}}) - E(\vec{s}_{\text{old}})}{T}). \tag{3.6}$$

   Otherwise it is rejected.

6. The temperature is decreased exponentially. The starting temperature is the mean change in the objective function (computed in the initialization phase).

7. If there is no acceptance for a larger number of steps (this number is adjustable), then the algorithm switches to the next digit and begins anew.

Having introduced the heuristics, we first have to show that the global minimum can be found from an arbitrary starting point. We thus choose a tight-binding band structure, which we try to reconstruct from its energy values at five symmetry points. We choose as an example the stochiometric TiO with rocksalt structure, which is another structure not yet tested above.

Table 3.1: TiO structure parameters

structure	fcc
lattice parameter a	4.181 Å from [67]

A tight-binding description for the substance can be found in [46]. The description takes second nearest neighbors into account. The parameters are:

Table 3.2: TiO tight-binding parameters from Mattheiss [46]

parameter	value (Ry)
E_s	−1.1027
$ss\sigma$	−0.0086
E_p	−0.0370
$pp\sigma$	+0.0179
$pp\pi$	−0.0044
E_d	+0.7979
$dd\sigma$	−0.0569
$dd\pi$	+0.0294
$dd\delta$	−0.0047
$sp\sigma$	0.0000
$sd\sigma$	+0.0509
$pd\sigma$	−0.1235
$pd\pi$	+0.0566

Figure 3.1: Band structure of TiO, parameters from Mattheiss

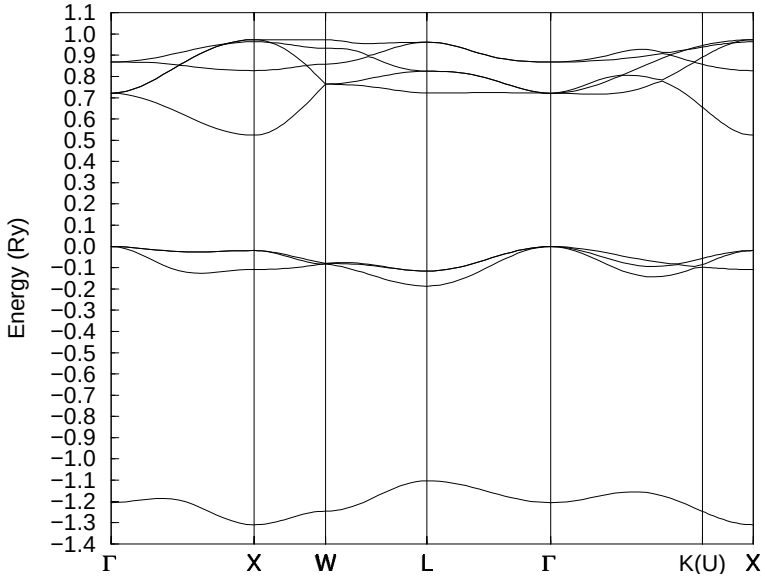

Figure 3.2: DOS of TiO, parameters from Mattheiss

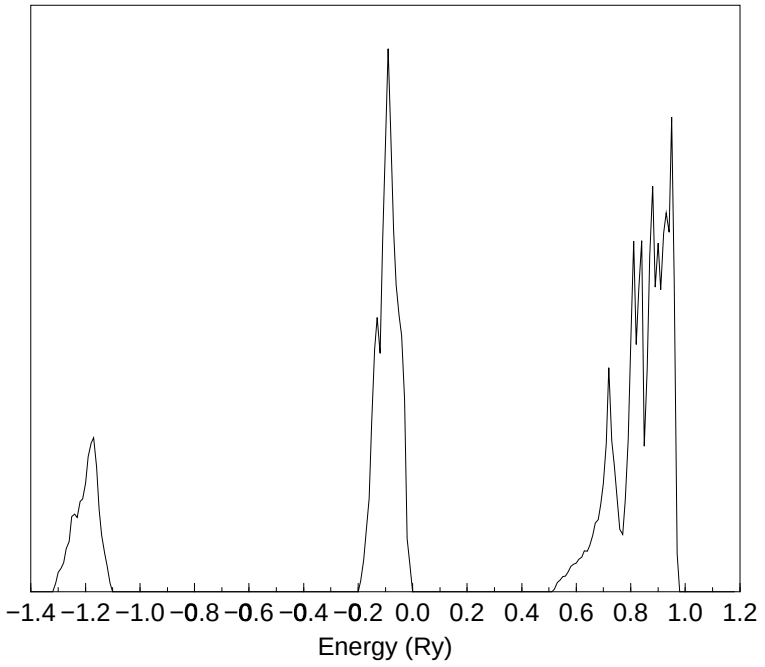

Now we will reconstruct this LCAO band structure only from the energy values at the high symmetry points in the Brillouin zone and assume that we ignore the parameter values altogether. The program needs as input the fit points:

Table 3.3: The input file for fitting the TiO LCAO bands (Mattheiss)

```
*These are the symmetry points for fitting:
*G , X , W , L , K(=U)
5.000
9.000
0.000 0.000 0.000 ENERGIES: -1.206 -0.001 -0.001 -0.001 0.721 0.721 0.721 0.868 0.868
0.000 0.000 1.504 ENERGIES: -1.310 -0.109 -0.019 -0.019 0.524 0.827 0.963 0.973 0.973
0.000 -0.752 1.504 ENERGIES: -1.246 -0.083 -0.080 -0.079 0.764 0.764 0.858 0.933 0.973
0.752 -0.752 0.752 ENERGIES: -1.103 -0.187 -0.116 -0.116 0.722 0.826 0.826 0.962 0.962
1.128 1.128 0.000 ENERGIES: -1.247 -0.097 -0.086 -0.056 0.655 0.857 0.891 0.939 0.946
```

The first number gives the number of fit points in $\vec{k}$-space, and the second number is the number of energy values at each fit point.

In the following plots the reconstructed band structure is shown after 0, 4000, 4500 and 10000 steps. The stars, respectively the dotted lines, denote the exact LCAO band structure.

Table 3.4: Progression in fitting the band structure of TiO

steps	0	4000	4500	15000	exact
distance	4.373693	0.204864	0.051647	0.000647	0.000000
$ss\sigma$	−1.0000	−0.0268	−0.0010	−0.0086	−0.0086
$sp\sigma$	+1.0000	+0.0000	+0.0000	+0.0000	+0.0000
$pp\sigma$	+1.0000	+0.0598	+0.0287	+0.0181	+0.0179
$pp\pi$	−1.0000	−0.0058	−0.0159	−0.0045	−0.0044
$sp\sigma$	−1.0000	−0.0917	−0.0558	−0.1689	−0.1691
$pd\sigma$	−1.0000	−0.2040	−0.1298	−0.1235	−0.1235
$pd\pi$	+1.0000	+0.1053	+0.0153	+0.0564	+0.0566
$dd\sigma$	−1.0000	−0.1121	−0.0462	−0.0569	−0.0569
$dd\pi$	+1.0000	+0.0661	+0.0189	+0.0294	+0.0294
$dd\delta$	−1.0000	−0.0600	−0.0046	−0.0047	−0.0047
E_s(O)	−1.0000	−1.3268	−1.2965	−1.1033	−1.1027
E_p(O)	−1.0000	−0.0025	−0.0410	−0.0374	−0.0370
E_d(Ti)	+1.0000	+0.7653	+0.8215	+0.7978	+0.7979

Figure 3.3: Band structure of TiO, fit after 0 steps

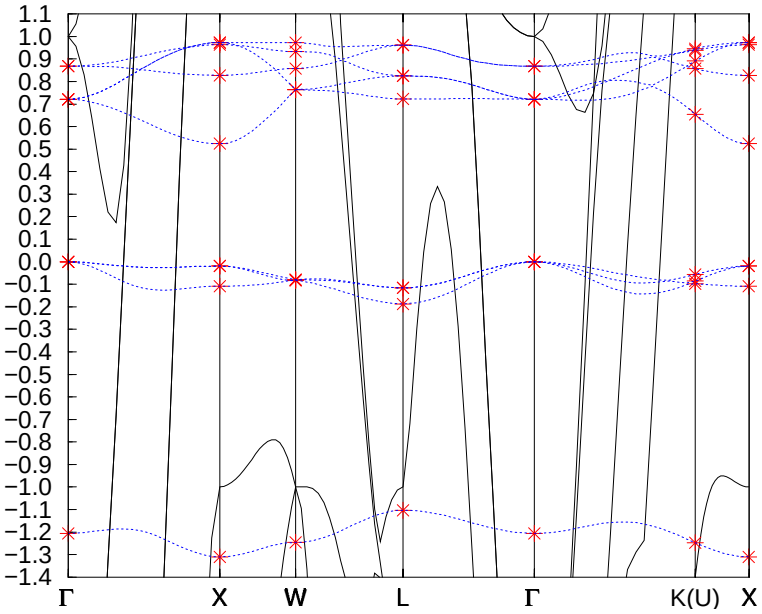

Figure 3.4: Band structure of TiO, fit after 4000 steps

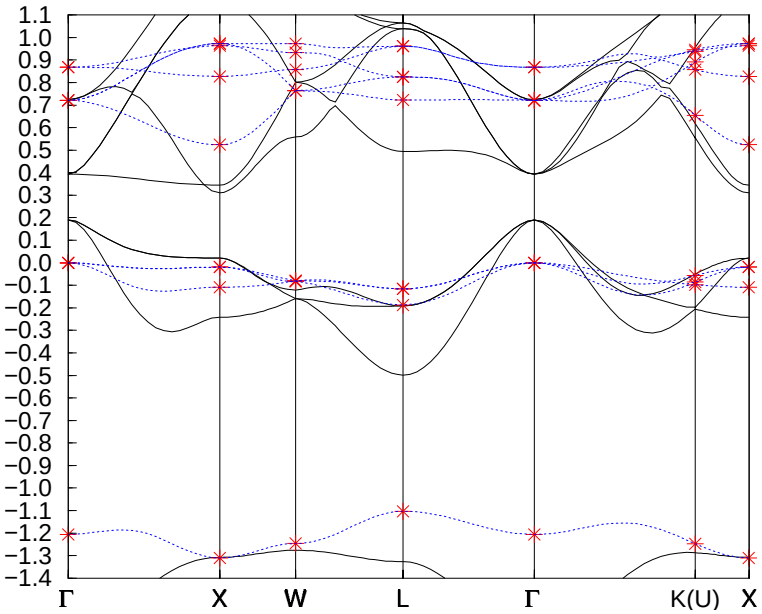

Figure 3.5: Band structure of TiO, fit after 4500 steps

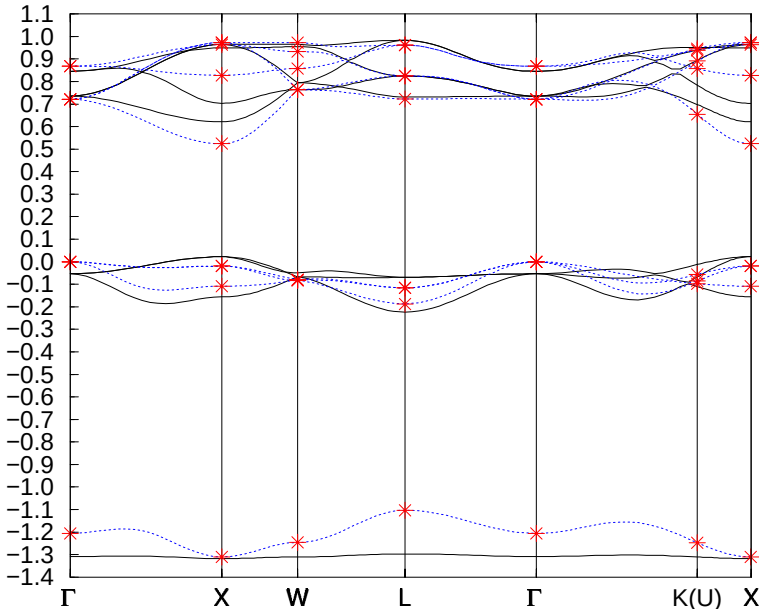

Figure 3.6: Band structure of TiO, fit after 15000 steps

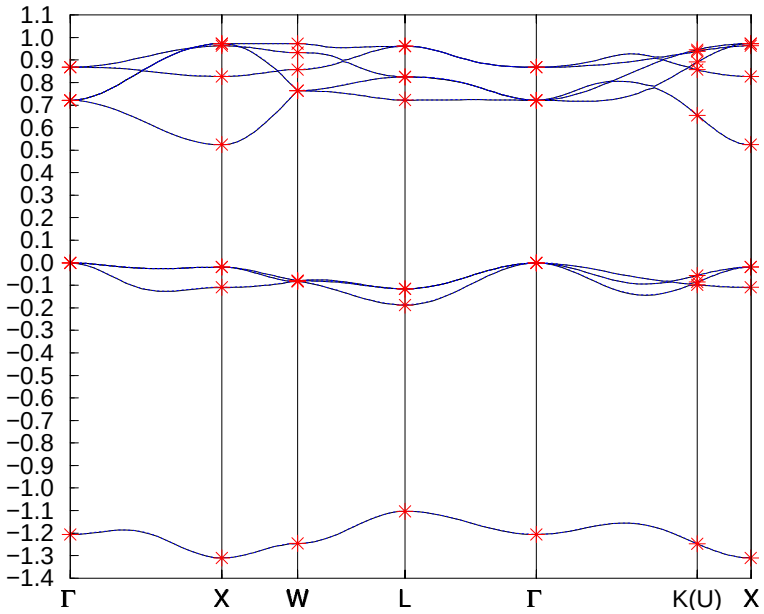

The progression for the optimized distance is shown in the following plot:

Figure 3.7: Progression for the TiO fitting, distance versus steps

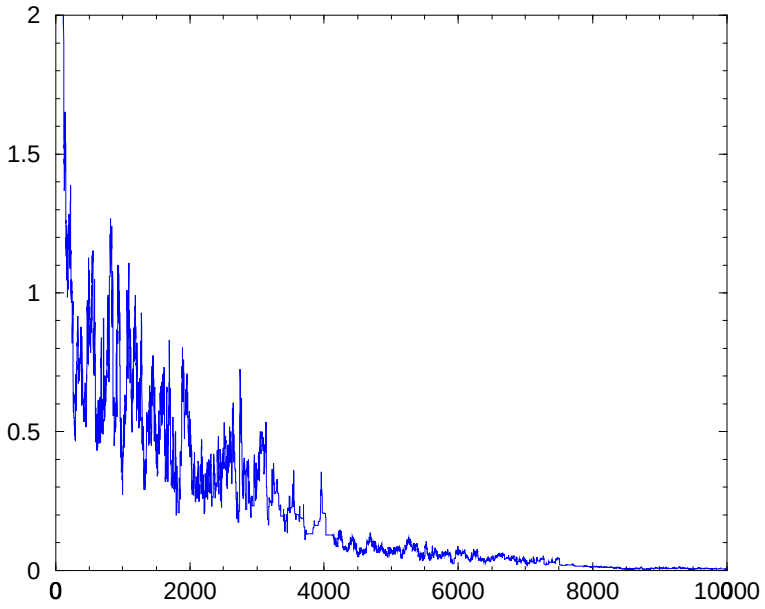

As we can see, the optimized distance becomes smaller in time and the variance of the optimized distance is diminishing. This can be explained as follows. The algorithm, which can be regarded as a random walker in the parameter space, starts with a large step size. This makes the random walker fast, but he sees the cost function on a coarse scale. Because the step size is large, every step may imply a large change in the function to be optimized, even if the function is very smooth. This in turn causes the large variance at the beginning. After approximately 4000 and 8000 steps the algorithm makes a switch to a smaller step size and the variance decreases. This bounds the random walker longer to the formerly found optimum area in the parameter space, which he can see now with a higher resolution. The crucial point in simulated annealing is of course the acceptance probability in case of a

deterioration in the cost function. This acceptance is controlled by the mean change in the cost function, and the temperature, whose evolution is shown in the following plot:

Figure 3.8: Mean change in the distance function and temperature versus steps in fitting TiO

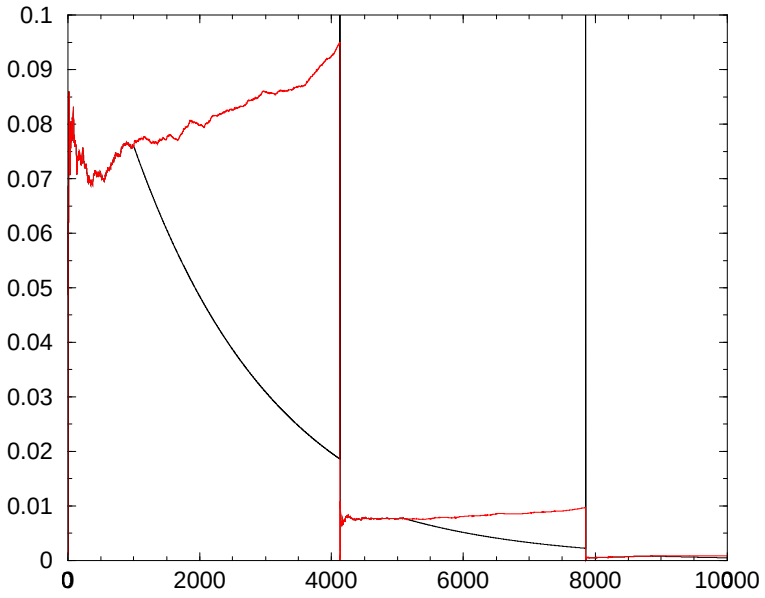

As we can see, the algorithm is able to find the global minimum and hence to reconstruct the LCAO band structure, starting from an arbitrary parameter vector.

3.1.2 Examples for the fitting strategy

In the above case, we have fitted a LCAO band structure by a LCAO band structure. Thus it was possible to reconstruct the total band structure to any desired accuracy. If we fit a band structure which was computed via another approach, e.g., APW, LMTO, etc., we should not expect that a

totally identical band structure will result. Furthermore, one should keep in mind that the finding of the correct band structure is by itself not an optimization task. The finding of the global minimum does not guarantee that this minimum represents the correct electronic structure. To illustrate this, we will fit in the following the empirical pseudopotential band structure for silicon [65]. The fitting points are:

Table 3.5: The input file for fitting the Si band structure

```
*For the data see: Papaconstantopoulos (page 263).
*Symmetry points are:
*G , X , L , W
4.000
8.000
0.000 0.000 0.000 ENERGIES: -12.599 0.000 0.000 0.000 3.413 3.413 3.413 4.464
1.157 0.000 0.000 ENERGIES: -8.363 -8.363 -3.079 -3.079 1.221 1.221 12.230 12.230
0.579 0.579 0.579 ENERGIES: -10.260 -7.351 -1.294 -1.294 2.214 3.984 3.984 8.751
1.157 0.579 0.000 ENERGIES: -8.201 -8.201 -4.009 -4.009 4.903 4.903 5.932 5.932
```

If we let our fitting algorithm roam freely in the parameter space, we will get after 30000 steps the following result:

Figure 3.9: Band structure fit for Si after 30000 steps

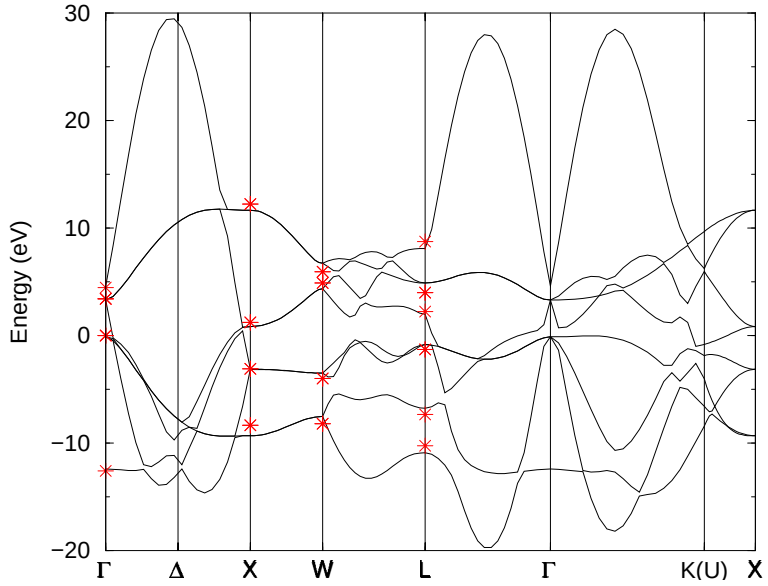

The parameters found at the minimum are by no means capable to reproduce the electronic structure of silicon. A closer look at the parameters reveals that they are not even consistent with the simplest physical demands one has for the hopping elements.

Table 3.6: Parameters from silicon band structure fit

steps	30000
distance	0.542918
$(ss\sigma)_1$	+3.2778
$(sp\sigma)_1$	−0.3231
$(pp\sigma)_1$	+3.4816
$(pp\pi)_1$	−0.2406
$(ss\sigma)_2$	−0.2134
$(sp\sigma)_2$	−1.9439
$(pp\sigma)_2$	+0.5849
$(pp\pi)_2$	−0.1595
$(ss\sigma)_3$	−0.3826
$(sp\sigma)_3$	−2.1758
$(pp\sigma)_3$	−2.2186
$(pp\pi)_3$	+0.8231
E_s(Si)	−1.3431
E_p(Si)	+0.5262

Some simple aspects concern the sign and the scaling law of a parameter with distance. We should expect the following signs [29], [84]:

Table 3.7: The signs for the parameters

parameter	sign
$ss\sigma$	$-$
$sp\sigma$	$+$
$pp\sigma$	$+$
$pp\pi$	$-$

Because we are interested in reproducing the results obtained by Papaconstantopoulos, we force the algorithm to obey the signs for the parameters from Papaconstantopoulos. These are:

Table 3.8: The signs for silicon according to Papaconstantopoulos [65]

parameter	first	second	third
$ss\sigma$	$-$	$+$	$+$
$sp\sigma$	$+$	$-$	$+$
$pp\sigma$	$+$	$+$	$-$
$pp\pi$	$-$	$-$	$+$

For the scaling law, we expect at least that the absolute value of the parameter should monotonically decrease to zero as the distance increases. With the signs from table 3.8, and obeying a very simple qualitative scaling law (for the second neighbor $(sp\sigma)_2$, we demand also a simple quantitative

scaling)

$$
\begin{aligned}
|(ss\sigma)_1| &> |(ss\sigma)_2| > |(ss\sigma)_3| \\
0.2\,|(sp\sigma)_1| &> |(sp\sigma)_2| > |(sp\sigma)_3| \\
|(pp\sigma)_1| &> |(pp\sigma)_2| > |(pp\sigma)_3| \\
|(pp\pi)_1| &> |(pp\pi)_2| > |(pp\pi)_3|
\end{aligned}
$$

one gets the following fit:

Figure 3.10: Band structure fit for Si after 30000 steps with constraints

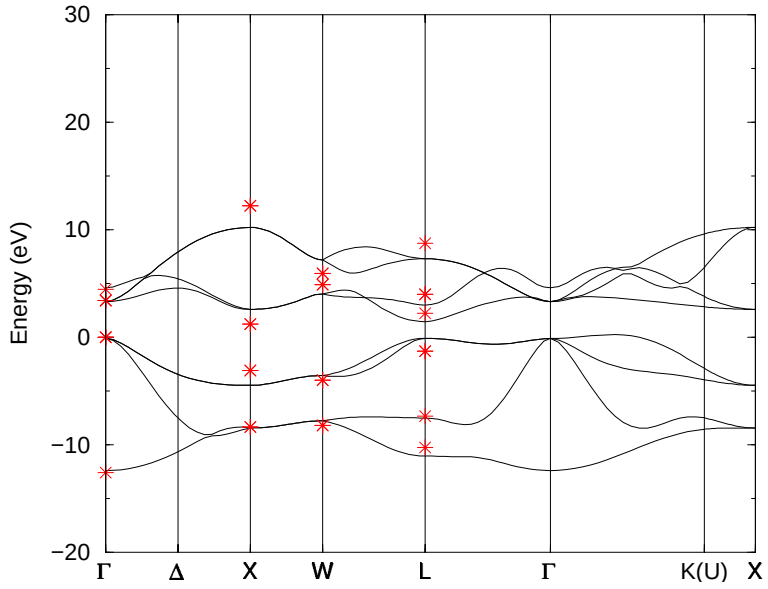

Table 3.9: Parameters from the band structure fit for Si with constraints

steps	30000
distance	1.112539
$(ss\sigma)_1$	−2.2373
$(sp\sigma)_1$	+2.2872
$(pp\sigma)_1$	+3.4662
$(pp\pi)_1$	−0.7534
$(ss\sigma)_2$	+0.0387
$(sp\sigma)_2$	−0.3499
$(pp\sigma)_2$	+0.7071
$(pp\pi)_2$	−0.3414
$(ss\sigma)_3$	+0.0372
$(sp\sigma)_3$	+0.0011
$(pp\sigma)_3$	−0.7061
$(pp\pi)_3$	+0.2412
E_s(Si)	−4.3717
E_p(Si)	+1.5056

While the distance is much greater for this fit, the result shows the band structure for silicon essentially correctly. The only incorrect result can be seen at position L. Here we see that bands five and six have been interchanged. This is mostly due to the parameters for the second and third neighbor

coupling, as we can learn if we omit the second and third neighbors.

Figure 3.11: Band structure for silicon, parameters from table 3.9, but only coupling to first nearest neighbors

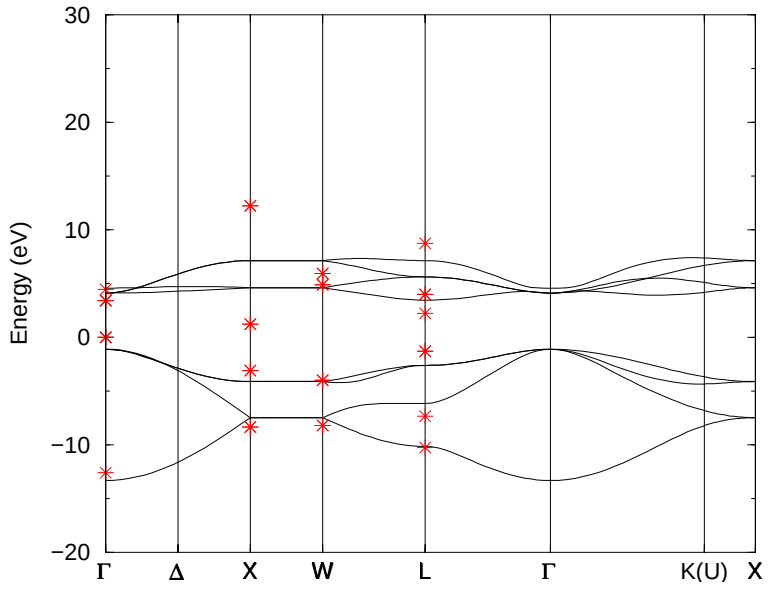

We see further that the fitting for the higher bands is worse than for the low lying bands, which is a well known shortcoming in the tight-binding approach. To take this into account, we introduce a weight factor of four for the bands 1-6 to force the algorithm to handle these bands more exactly.

Figure 3.12: Band structure fit for Si after 30000 steps with constraints, and weights

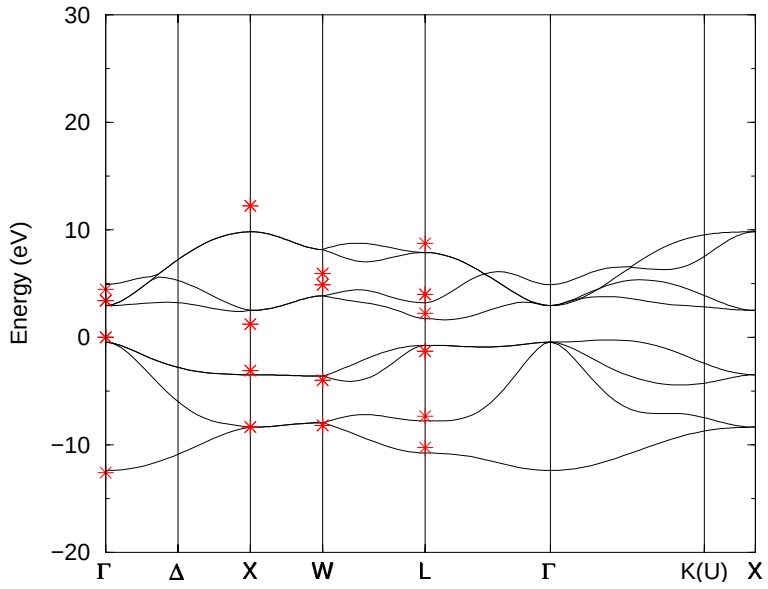

This band structure is very similar to the band structure obtained from an empirical pseudopotential calculation [65]. For this band structure Papaconstantopoulos has also given a LCAO fit. We compare our parameters to those of Papaconstantopoulos:

Table 3.10: Parameters from band structure fit for Si

steps 30000 distance 1.481891		
parameter	our fit	fit ref. [65]
$(ss\sigma)_1$	−2.1665	−2.3623
$(sp\sigma)_1$	+2.0800	+1.8640
$(pp\sigma)_1$	+3.6125	+2.8588
$(pp\pi)_1$	−0.8574	−0.9469
$(ss\sigma)_2$	+0.1078	+0.1360
$(sp\sigma)_2$	−0.3416	−0.2638
$(pp\sigma)_2$	+0.5458	+0.4101
$(pp\pi)_2$	−0.3414	−0.1370
$(ss\sigma)_3$	+0.0017	+0.0460
$(sp\sigma)_3$	+0.0001	+0.1943
$(pp\sigma)_3$	−0.3225	−0.0526
$(pp\pi)_3$	+0.0575	+0.0808
E_s(Si)	−5.0436	−5.1928
E_p(Si)	+1.7993	+1.0583

For a better comparison, we show both band structures in one plot:

Figure 3.13: Band structure fit for Si, solid line: present fit, dashed line: ref. [65].

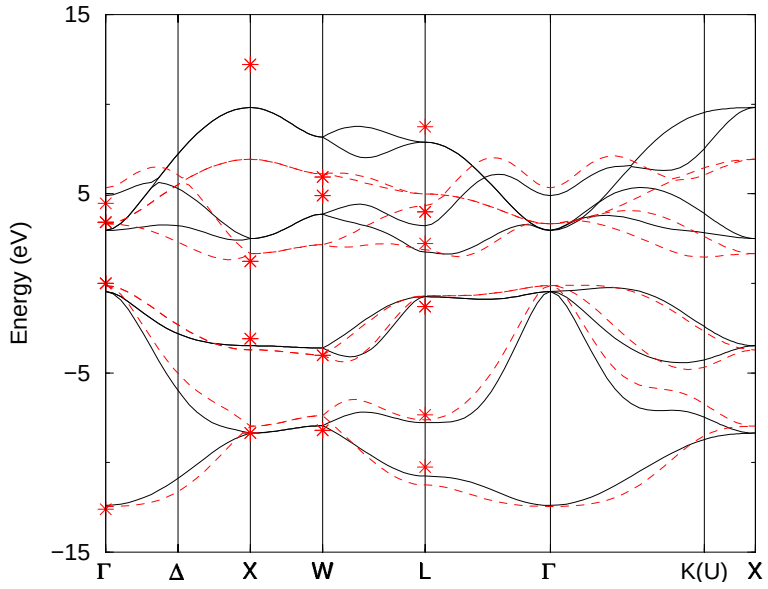

The total cost in computing time on a DEC alpha workstation is approximately 30 minutes, which is much faster than the genetic algorithm of [83].

3.2 Conclusion

These two sets of results are in a remarkably good agreement, in particular if one considers that we have used only four fit points in contrast to Papaconstantopoulos, who has used 33 fit points, which allows for a much better guidance of the bands. But these were not available in the literature. The second aspect is that our method is much simpler to apply. It works in general for simple systems as well as for complex systems. To appreciate our approach, we outline the fitting approach, taken by Papaconstantopoulos [65], for the very simple silicon system. As we will see, even for this

simple system, the effort to find good starting values, which are absolute necessary here, and then finding the 'physical minimum' is demanding. To find the needed starting parameters, we treat the problem in its three center formulation first, because the set-up is more easy in the three center formalism. The starting values are found from approximating linear equations for the problem, which demands a block diagonalization of the eight times eight hamiltonian at some special high symmetry points in the Brillouin zone, a task, which is of course only possible for a simple matrix. These equations are:

$$E(\Gamma_1) = E_{s,s}(000) + 4E_{s,s}(\frac{1}{2}\frac{1}{2}\frac{1}{2}) + 12E_{s,s}(110) \tag{3.7}$$

$$E(\Gamma_{2'}) = E_{s,s}(000) - 4E_{s,s}(\frac{1}{2}\frac{1}{2}\frac{1}{2}) + 12E_{s,s}(110) \tag{3.8}$$

$$E(\Gamma_{15}) = E_{x,x}(000) + 4E_{x,x}(\frac{1}{2}\frac{1}{2}\frac{1}{2}) + 8E_{x,x}(110) + 4E_{x,x}(011) \tag{3.9}$$

$$E(\Gamma_{25'}) = E_{x,x}(000) - 4E_{x,x}(\frac{1}{2}\frac{1}{2}\frac{1}{2}) + 8E_{x,x}(110) + 4E_{x,x}(011) \tag{3.10}$$

$$E(X_3) = E_{x,x}(000) + 4E_{x,y}(\frac{1}{2}\frac{1}{2}\frac{1}{2}) - 4E_{x,x}(011) \tag{3.11}$$

$$E(X_4) = E_{x,x}(000) - 4E_{x,y}(\frac{1}{2}\frac{1}{2}\frac{1}{2}) - 4E_{x,x}(011) \tag{3.12}$$

To solve the above system of simultaneous equations, the additional approximation of setting the parameters $E_{s,s}(\frac{1}{2}\frac{1}{2}\frac{1}{2})$ and $E_{x,x}(110)$ equal to zero is made.

Then the solution reads:

$$E_{s,s}(000) = \frac{1}{2}[E(\Gamma_1) + E(\Gamma_{2'})] \tag{3.13}$$

$$E_{x,x}(000) = \frac{1}{4}[E(\Gamma_{15}) + E(\Gamma_{25'}) + E(X_3) + E(X_4)] \tag{3.14}$$

$$E_{s,s}(\frac{1}{2}\frac{1}{2}\frac{1}{2}) = \frac{1}{8}[E(\Gamma_1) - E(\Gamma_{2'})] \tag{3.15}$$

$$E_{x,x}(\frac{1}{2}\frac{1}{2}\frac{1}{2}) = \frac{1}{8}[E(\Gamma_{15}) - E(\Gamma_{25'})] \tag{3.16}$$

$$E_{x,y}(\frac{1}{2}\frac{1}{2}\frac{1}{2}) = \frac{1}{8}[E_(X_3) - E(X_4)] \tag{3.17}$$

$$E_{x,x}(011) = \frac{1}{16}[E(\Gamma_{15}) + E(\Gamma_{25'}) - E(X_3) - E(X_4)] \tag{3.18}$$

Thus one gets seven out of 13 three-center parameters corresponding to first- and second-neighbor interactions. To determine all 13 parameters a least-squares program is used. The encoding of a standard least-squares fit algorithm demands again a substantial programming effort. The next step is to add the seven additional third-neighbor interaction parameters and go through the least-squares program again to find all 20 parameters. Finally, utilizing the relations between three- and two-center integrals, Papaconstantopoulos obtains estimates for the starting parameters for the two-center fit. The fitting is done for 33 k-points for all eight bands. The higher number of k-points allows a much better guidance of the bands. But if we consider the fact that an experimentalist will only have a few values, which he has measured at high symmetry points, it is of great advantage to get a good fit from only four or five k-points. As we have seen, this is possible with our annealing algorithm. The only choice left to the user is the weight function for the distance. Here no recipes can be given.

Chapter 4

The scaling laws for the hopping integrals

While we were able to reproduce very well a given band structure in the section above, one point remains to be solved. Looking at the parameters in the book of Papaconstantopoulos, but also in many other papers, we see that the parameters exhibit different scaling laws with distance, and obey different sign rules. This is in contrast to our simple physical intuition, which demands that the hopping matrix elements decay steadily and do not change sign for distances close to or greater than the nearest-neighbor distance. Looking at tight-binding theory in the context of density functional theory confirms our intuition [20], [21], [69]. To summarize these investigations, we can state that our parameters should obey some more or less prescribed simple scaling laws without sign change. The absolute form of these laws, and their transferability to different substances, is a hotly debated topic in tight-binding theory [66], [53], [25], [49], [18], [75], [9], [10], [50], [3], [41], [52], [85].

In the following we will see that it is possible to find scaling laws for the

hopping parameters, which fulfill three basic postulates:

1. The sign of the hopping matrix elements comply with the basic assumptions of tight-binding theory.

2. The hopping matrix elements decay steadily with distance and do not change sign for distances close to or greater than the nearest-neighbor distance.

3. The scaling laws for the hopping matrix element should allow for transferability. This is to say that it must be possible to extrapolate to substances or substance properties, which have not been taken into account in the fitting.

With the help of our general tight-binding and fitting program, it is relatively simple to find such scaling laws under very mild conditions. We will construct reasonable band structures from only four or five fit points, without the assumption of any special quantitative scaling laws, and without the faintest idea of tight-binding theory. This is to the best of the author's knowledge in contrast to the currently available programs. These programs require a much deeper theoretical background of the user, they are not general, and need many more fit points. But it is this universality, which makes a program useful in the field of practical applications, where one wants to know the most important electronic features of a solid, without spending much time in theory and programming, and where one only has a few measured values at hand.

4.1 The sign for the parameters

To determine the sign of a hopping matrix element, we only have to remember basic Hückel molecular orbital (HMO) theory [32], [84]. The orthogonal two center tight-binding approach can be interpreted in terms of the simple hydrogen molecule, which forms the paradigm for the two center bonding. We assume that we can write the Hamilton operator as:

$$H = -\frac{\hbar^2\nabla^2}{2m} + V_1(\vec{r}) + V_2(\vec{r}), \tag{4.1}$$

with $V_1(\vec{r})$ and $V_2(\vec{r})$ the potentials on atom one and two. Hence we write for H_{12} :

$$H_{12} = \langle 1| - \frac{\hbar^2\nabla^2}{2m} + V_1(\vec{r}) + V_2(\vec{r})|2\rangle \tag{4.2}$$

$$= \langle 1| - \frac{\hbar^2\nabla^2}{2m} + V_2(\vec{r})|2\rangle + \langle 1|V_1(\vec{r})|2\rangle \tag{4.3}$$

$$= E_2\langle 1|2\rangle + \langle 1|V_1(\vec{r})|2\rangle \tag{4.4}$$

Because we assume orthogonality for our basis, we have:

$$H_{12} = \langle 1|V_1(\vec{r})|2\rangle \tag{4.5}$$

The sign of H_{12} is therefore determined by the sign of the orbital lobes of $\langle 1|$ and $\langle 2|$, and of the potential, which is attractive , i.e. negative. E.g., for the $pp\sigma$ integral, we get a positive sign. In total we obtain the following sign rules:

Table 4.1: The signs for the parameters

parameter	sign
$ss\sigma$	$-$
$sp\sigma$	$+$
$pp\sigma$	$+$
$pp\pi$	$-$

4.2 The scaling laws

While it was very simple to derive the appropriate signs for the hopping matrix elements, it is much harder to find transferable scaling laws. To make a first step, we remember chapter 2.5, pages 42 – 45. There we have seen that the scaling laws given by Harrison are not bad at all when compared to the results of Mattheiss, who has fitted his APW band structure. Representing Mattheiss's values by polynomials, we have seen that the curvature of these polynomials was often approximately the same as the curvature of Harrison's scaling laws. They were incorrect only as there is an absolute shift in energy. Therefore it seems reasonable to keep Harrison's scaling laws in a slightly modified form, and only to adjust the energies. This approach is taken, e.g., in [18], [85]. Here the dd-scaling is given by the authors as:

$$dd\sigma = -6W(\frac{2}{5})(\frac{S}{r})^5 \tag{4.6}$$

$$dd\pi = +4W(\frac{2}{5})(\frac{S}{r})^5 \tag{4.7}$$

$$dd\delta = -1W(\frac{2}{5})(\frac{S}{r})^5, \tag{4.8}$$

where S is the Wigner-Seitz radius, and W is the nominal bandwidth. In fitting to the actual bandwidth the approach is not able to produce high quality tight-binding band structures. To get the full flexibility, we can assume a standard fit function, e.g., an ordinary polynomial [75], a Chebychev polynomial, or a cubic spline [41]. Increasing the order of the polynomials makes the fit better. In ref. [21] the authors used Chebychev polynomials of order 12 to fit the matrix elements. A fit function, which is intermediate between these two approaches, rests upon the following consideration. Most scaling laws we find in nature are of exponential or power law form. It is therefore natural to assume for the form of the fit function a mixture of exponential and power law terms. In ref. [50] we find the following proposal:

$$H(r) = A_1 r^{B_1} e^{-C_1 r} + A_2 r^{B_2} e^{-C_2 r}, \tag{4.9}$$

where A and B are to be fitted and C is prescribed. In ref. [9], [53] we find a similar suggestion:

$$H(r) = (\alpha + \beta r + \gamma r^2) e^{-\delta^2 r} f(r) \tag{4.10}$$

with

$$f(r) = \frac{1}{\exp[(r - r_0)/l] + 1}, \tag{4.11}$$

where $f(r)$ is a universal cutoff function chosen to simplify the calculation (with r_0 and l prescribed.)

Each of these suggestions leads to high quality results in the band structure. Examples for calculations can be found in [70], [57], [54], [90]. The data presented there rest upon a large data base of information. To obtain these data, very often a fit to first principle computations for small clusters has been done, and then the results of these computations have been reproduced by their tight-binding analogue. As a matter of fact this approach needs a

substantial computational effort to set up the needed data base, and requires an enormous amount of data for input. But what is to be done, if one is not in the fortunate situation to have access to such a data base, or if one is an experimentalist, who normally has at his disposal only few measurements? Is it possible to get reasonable results, even in such a precarious situation? As we will see, the answer is a restricted yes.

4.2.1 The minimal qualitative scaling

In the previous section, we have seen that each fit was done for a special scaling law. The choice of such a scaling law depends on theoretical knowledge, experience, and numerical purposes. Here we will raise the question, to what extent we can minimize the information on the scaling law and the data, and nonetheless get reasonable results. The answer to the question is intriguingly simple. The signs of the parameters and a pure qualitative scaling is sufficient. We will show this for the paradigma silicon. Endowed with only four fit points, the correct signs, and a pure qualitative scaling law

$$|(ss\sigma)_1| > |(ss\sigma)_2| > |(ss\sigma)_3|$$
$$|(sp\sigma)_1| > |(sp\sigma)_2| > |(sp\sigma)_3|$$
$$|(pp\sigma)_1| > |(pp\sigma)_2| > |(pp\sigma)_3|$$
$$|(pp\pi)_1| > |(pp\pi)_2| > |(pp\pi)_3|$$

our search algorithm supplies us with the following band structure:

Figure 4.1: Band structure fit for Si

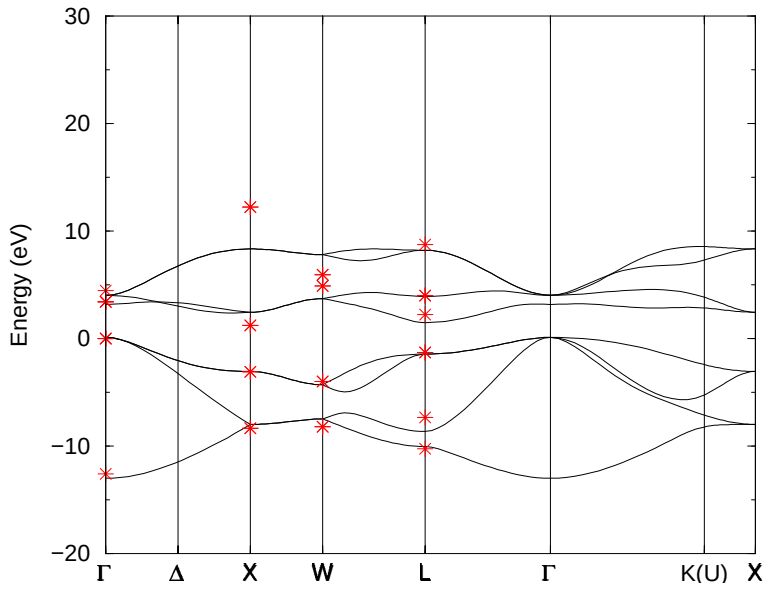

Table 4.2: Parameters from the band structure fit for Si with minimal input

steps	57000
distance	1.8557
$(ss\sigma)_1$	−1.9877
$(sp\sigma)_1$	+2.1150
$(pp\sigma)_1$	+3.6500
$(pp\pi)_1$	−0.8037
$(ss\sigma)_2$	−0.0175
$(sp\sigma)_2$	+0.0494
$(pp\sigma)_2$	+0.6292
$(pp\pi)_2$	−0.2575
$(ss\sigma)_3$	−0.0116
$(sp\sigma)_3$	+0.0027
$(pp\sigma)_3$	+0.0229
$(pp\pi)_3$	−0.1071
E_s(Si)	−4.7043
E_p(Si)	+1.6067

The valence bands are correctly reproduced. There is only a bias at L_1. The higher lying conduction bands are not as well represented as the valence bands. But this is a general failure of tight-binding theory, when one uses only a minimal basis. Here it is of much greater importance to notice the fact that

we have obtained our band structure in the interesting region, i.e. the valence bands and the first two conduction bands, from very little information. This becomes more obvious if we compare our results to other computations and experimental data [3]. These computations are:

- The approach taken by Frauenheim and coworkers [4], [21], who are working with a nonorthogonal two center formalism. All the needed hopping

$$H_{ij} = \langle \Phi_i | H | \Phi_j \rangle \tag{4.12}$$

  and overlap

$$S_{ij} = \langle \Phi_i | \Phi_j \rangle \tag{4.13}$$

  integrals are computed explicitly. The $|\Phi_i\rangle$ are eigenfunctions from DFT/LDA calculations of a single atom in a confining potential. The approach is denoted as DF-TB.

- The approach taken by Menon and Subbaswamy [57], [56], [55], denoted as MS-TB.

- The approach taken by Bernstein and Kaxiras [3], which is a modification of the MS-TB approach. This approach is denoted as NO-TB.

- Our approach which fits to a few given values on a minimal information base. The approach is denoted as MIN-TB.

Table 4.3: Comparison of experiment and theory for different approaches

	DFT/LDA	NO-TB	MS-TB	DF-TB	MIN-TB	Exp.
Valence band width	11.92	11.75	13.83	10.69	13.1	
Band gap at Γ	3.15	1.68	3.07	3.20	3.1	2.74[a]
Minimum band gap	1.14	1.51	2.72	3.20	1.38	1.17[b]

[a]Ref. [87]
[b]Ref. [73]

At first glance, one would say that the DFT/LDA results are in excellent agreement with experiment. A closer look reveals that this is not the case. DFT/LDA underestimates the band gap systematically of about one eV. To compensate this systematic error, a so called scissor-operator is introduced, which is nothing else than an appropriately chosen numerical constant, to widen the gap [19], [2], [13]. The DFT/LDA results in table 4.3 include a 0.6 eV scissor-operator shift of the conduction levels [19], [2]. Taking the scissor-operator into account, we find that the MIN-TB approach supplies the best description for the most important features of the band-structure. A more detailed picture concerning experiment and MIN-TB shows the following table:

Table 4.4: Comparison of experiment, empirical pseudopotential, and MIN-TB

Position	Experiment	Pseudopotential (empirical)[Ref. 65]	minimal fit
Γ_1	-12.4 ± 0.6[Ref. 27]	-12.6	-13.0
	-12.5 ± 0.6[Ref. 42]		
Γ_{15}		$+3.4$	$+3.2$
$\Gamma_{2'}$		$+4.5$	$+4.0$
Γ_{25}		0.0	$+0.1$
Σ_1	-4.7 ± 0.2[Ref. 27], [42]		-3.6
	-4.4[Ref. 80]		
X_1		-8.4	-8.0
X_1		$+1.2$	$+2.5$
X_3		$+12.2$	$+8.3$
X_4	-2.5 ± 0.3[Ref. 42]	-3.1	-3.1
	-2.9[Ref. 80]		
$L_{2'}$	-9.3 ± 0.4[Ref. 42]	-10.3	-10.0
$L_{2'}$		$+8.8$	$+8.2$
L_1	-6.4 ± 0.4[Ref. 27]	-7.4	-8.7
	-6.8 ± 0.2[Ref. 42]		
L_1		$+2.2$	$+1.5$
$L_{3'}$	-1.2 ± 0.2[Ref. 80]	-1.3	-1.5
L_3		$+4.0$	$+4.0$
W		-8.2	-7.5
W		-4.0	-4.3
W		$+4.9$	$+3.7$
W		$+5.9$	$+7.8$

If we demand 'better' results, we must extend our knowledge about silicon, i.e., we need more input data in the form of more fit points, to ensure a better guidance of the bands. To become more flexible, we could increase the coupling range.

4.3 Conclusion

Summarizing the last results, we can say:

1. Our approach supplies a reasonable band structure, and estimates for the main electronic features, such as the band gap and the valence band width on a very restricted basis of information.

2. Looking at table 4.3, we see, that the results are in excellent agreement with experiment.

3. The theoretical basis is reduced to its minimum. We only need the correct sign rules, and a minimal scaling law. This makes the software nearly universal.

4. The time needed to get the results for Si is on a modern Pentium computer of about 60 min.

In this work, we will not address the question of transferability, because to this purpose, three more steps have to be taken. This is the compilation of an extended data base for different silicon clusters on the basis of first principle methods, a fitting to this data base, and then the extrapolation to properties which can only be explained on a mesoscopic scale, e.g., attributes which can be computed with the help of molecular dynamics, etc. However it should be pointed out that the fitting procedure proposed here is the proper tool to approach this problem.

List of Figures

List of Tables

Bibliography

[1] A.L. Ames, D.R. Nadeau, and J.L. Moreland. *VRML 2.0 Sourcebook*. John Wiley & Sons, 1997.

[2] G.A. Baraff and M. Schlüter. Migration of interstitials in silicon. *Phys. Rev. B*, 1984.

[3] N. Bernstein and E. Kaxiras. Nonorthogonal tight-binding hamiltonians for defects and interfaces in silicon. *Phys. Rev. B*, 56(16):10488–10496, 1997.

[4] P. Blaudeck, Th. Frauenheim, D. Porezag, and E. Seifert, G. Fromm. A method and results for realistic molecular dynamic simulation of hydrogenated amorphous carbon structures using a scheme consisting of a linear combination of atomic orbitals with the local-density approximation. *J. Phys.: Condens. Matter*, 4:6389–6400, 1992.

[5] J.K. Burdett. Electronic control of the geometry of rutile and related structures. *Inorg. Chem.*, 24:2244–2253, 1985.

[6] J.K. Burdett and T. Hughbanks. Aspects of metal-metal bonding in early-transition-metal dioxides. *Inorg. Chem.*, 24:1741–1750, 1985.

[7] D.J. Chadi and M.L. Cohen. Tight-binding calculations of the valence bands of diamond and zincblende crystals. *Phys. Stat. Sol. B*, 68:405–419, 1975.

[8] N.E. Christensen and A.R. Mackintosh. Electronic structure of cubic sodium tungsten bronze. *Phys. Rev. B*, 1987.

[9] R.E. Cohen, M.J. Mehl, and D.A. Papaconstantopoulos. Tight-binding total-energy method for transition and noble metals. *Phys. Rev. B Rapid Communications*, 50(19):14694–14697, 1994.

[10] R.E. Cohen, L. Stixrude, and E. Wasserman. Tight-binding computations of elastic anisotropy of Fe, Xe, and Si under compression. *Phys. Rev. B*, 56(14):8575–8589, 1997.

[11] N. Daud, C. Gout, and C. Jouanin. Electronic band structure of titanium dioxide. *Phys. Rev. B*, 15(6), 1977.

[12] M. Dorrer, R. Eibler, and A. Neckel. An improved LCAO interpolation scheme for energy band structures. Application to four compounds (ScN, ScP, TiN, ZrN) crystallizing in the sodium chloride structure. *Theoret. Chim. Acta(Berl.)*, 60:313–325, 1981.

[13] R.M. Dreizler and E.K.U. Gross. *Density functional theory.* Springer-Verlag, Berlin Heidelberg, 1990.

[14] H. Dücker. private communication.

[15] R.F. Egorov, B.I. Reser, and V.P. Shirokovskii. Consistent treatment of symmetry in the tight binding approximation. *Phys. Stat. Sol.*, 26:391, 1968.

[16] F. Ercolessi and J.B. Adams. Interatomic potentials from first-principles calculations: the force-matching method. *Europhys. Lett.*, 26(8):583–588, 1994.

[17] R.A. Evarestov and V.P. Smirnov. *Site symmetry in crystals*. Springer Series in Solid-State Sciences 108. Springer-Verlag, 1993.

[18] M.W. Finnis, A.T. Paxton, D.G. Pettifor, A.P. Sutton, and Y. Ohta. Interatomic forces in transition metals. *Phil. Mag. A*, 58(1):143–163, 1988.

[19] V. Fiorentini and A. Balderesschi. Dielectric scaling of the self-energy scissor operator in semiconductors and insulators. *Phys. Rev. B*, 51(23):17196–17198, 1995.

[20] W.M. Foulkes and R. Haydock. Tight-binding models and density-functional theory. *Phys. Rev. B*, 39(17):12520–12536, 1989.

[21] Th. Frauenheim, F. Weich, Th. Köhler, S. Uhlmann, D. Porezag, and G. Seifert. Density-functional-based construction of transferable nonorthogonal tight-binding potentials for Si and SiH. *Phys. Rev. B*, 52(15), 1995.

[22] S. Geman and D. Geman. Stochastic relaxation, Gibbs distribution and the Baysian restoration in images. *IEEE Trans. Patt. Anal. Mac. Int.*, 6(6):721–741, 1984.

[23] K.M. Glassford and J.R. Chelikowsky. Structural and electronic properties of titanium dioxide. *Phys. Rev. B*, 46(3):1284–1298, 1992.

[24] H. Gleitner. Nanostructured materials: State of the art and perspectives. *Nanostructured Materials*, 6:3–14, 1995.

[25] L. Goodwin, A.J. Skinner, and D.G. Pettifor. Generating transferable tight-binding parameters: application to silicone. *Europhys. Let.*, 9:701–706, 1989.

[26] C.M. Goringe, D.R. Bowler, and Hernández. Tight-binding modelling of materials. *Rep. Prog. Phys.*, 60:1447–1512, 1997.

[27] W.D. Grobman and D.E. Eastman. Photoemission valence-band densities of states for Si, Ge, and GaAs using synchrotron radiation. *Phys. Rev. Lett.*, 29:1508–, 1972.

[28] G.C. Hadjipanayis and R.W. Siegel, editors. *Nanophase Materials: Synthesis, Properties, Applications*. Kluwer Academic Publishers, Dordrecht, 1994.

[29] W.A. Harrison. *Electronic structure and the properties of solids*. Dover Publications, 1989.

[30] H.O. Hartley. The modified Gauss-Newton method for the fitting of non-linear regression functions by least squares. *Technometrics*, 3(2):269–280, 1961.

[31] H.-L. Hase. *Dynamische virtuelle Welten mit VRML 2.0*. IX Edition, 1997.

[32] E. Heilbronner and H. Bock. *Das HMO-Modell und seine Anwendung (Grundlagen und Handhabung)*. VerlagChemie, Weinheim, 2. edition, 1978.

[33] R. Hoffmann. *Solids and surfaces*. VCH, 1988.

[34] L. Ingber. Very fast simulated reannealing. *Mathematical and Computer Modelling*, 12(8):967–973, 1989.

[35] L. Ingber and B. Rosen. Genetic algorithms and very fast simulated reannealing: a comparison. *Mathl. Comput. Modelling*, 16(11):87–100, 1992.

[36] A.H. Kahn and A.J. Leyendecker. Electronic energy bands in Strontium Titanate. *Phys. Rev.*, 135(5A), 1964.

[37] W. Kinzel and G. Reents. *Physik per Computer*. Spektrum Akademischer Verlag, 1996.

[38] S. Kirkpatrick, C.D. Gelatt, and M.P. Vecchi. Optimization by simulted annealing. *Science*, 220:671–680, 1983.

[39] C. Kittel. *Introduction to solid state physics*. John Wiley & Sons, 3rd edition, 1966.

[40] L. Kopp, B.N. Harmon, and S.H. Liu. Band structure of cubic Na_xWO_3. *Solid State Communications*, 22:677–679, 1977.

[41] T.J. Lenosky, J.D. Kress, I. Kwon, and A.F. Voter. Highly optimized tight-binding model of silicon. *Phys. Rev. B*, 55(3):1528–1544, 1997.

[42] L. Ley, S. Kowalczyk, R. Pollak, and D.A. Shirley. X-ray photoemission spectra of crystalline and amorphous Si and Ge valence bands. *Phys. Rev. Lett.*, 29:1088–, 1972.

[43] P.-O. Löwdin. On the non-orthogonality problem connected with the use of atomic wave functions in the theory of molecules and crystals. *J.Chem.Phys.*, 18(3):365–375, 1950.

[44] P.-O. Löwdin. A note on the quantum-mechanical pertubation theory. *J.Chem.Phys.*, 19(11):1396, 1951.

[45] L.F. Mattheiss. Crystal-field effects in the tight-bonding approximation: ReO_3 and perovskite structures. *Phys. Rev. B*, 2(10):3918–3935, 1970.

[46] L.F. Mattheiss. Electronic structure of the 3d transition-metal monoxides. I Energy-band results. *Phys. Rev. B*, 5(2):290–306, 1972.

[47] L.F. Mattheiss. Electronic structure of $RuO_2, OsO_2,$ and IrO_2. *Phys. Rev. B*, pages 2433–2450, 1976.

[48] L.F. Mattheiss. Band properties of metallic corundum-phase V_2O_3. *J.Phys.: Condens. Matter 6*, pages 6477–6484, 1994.

[49] W. Matthew and C. Foulkes. Tight-binding models and density-functional theory. *Phys. Rev. B*, 39(17):12520–12536, 1989.

[50] A.K. McMahan and J.E. Klepeis. Direct calculation of Slater-Koster parameters: Fourfold-coordinated silicon/boron phases. *Phs. Rev. B*, 56(19):12250–12262, 1997.

[51] R. McWeeny. *Coulsons Chemische Bindung*. S. Hirzel Verlag, Stuttgart, 2nd edition, 1984.

[52] M.J. Mehl and D.A. Papaconstantopoulos. Applications of a new tight-binding method for transition metals: Manganese. *Europhys. Let.*, 31(9):537–541, 1995.

[53] M.J. Mehl and D.A. Papaconstantopoulos. Applications of a tight-binding total-energy method for transition and noble metals: elastic constants, vacancies, and surfaces of monatomic metals. *Phys. Rev. B*, 54(7):4519–4530, 1996.

[54] M. Menon and K.R. Subbaswamy. Universal parameter tight-binding molecular dynamics: Application to C_{60}. *Phys. Rev. Let.*, 67(25):3487–3490, 1991.

[55] M. Menon and K.R. Subbaswamy. Nonorthogonal tight-binding molecular-dynamics study of silicon clusters. *Phys. Rev. B*, 47(19):12754–12759, 1993.

[56] M. Menon and K.R. Subbaswamy. Transferable nonorthogonal tight-binding scheme for silicon. *Phys. Rev. B*, 50(16):11577–11582, 1994.

[57] M. Menon and K.R. Subbaswamy. Nonorthogonal tight-binding molecular-dynamics scheme for silicon with improved transferability. *Phys. Rev. B*, 55(15):9231–9234, 1997.

[58] N. Metropolis, A.W. Rosenbluth, M.N. Rosenbluth, A.H. Teller, and E. Teller. Equation of state calculations by fast computing machines. *J. Chem. Phys.*, 21(6):1087–1092, 1953.

[59] M. Miasek. Tight-binding method for hexagonal close-packed structure. *Rhys. Rev.*, 107(1), 1957.

[60] K.C. Mishra, K.H. Johnson, and P.C. Schmidt. A comparative study of the electronic structures of titanium dioxide and strontium titanate. *J. Phys. Chem. Solids*, 54(2):237–242, 1993.

[61] T.K. Mitra, S. Chatterjee, and G.J. Hyland. A method for obtaining parametrized bands of Rutile VO_2. *Can. J. Phys.*, 51:352, 1973.

[62] S. Munnix and M. Schmeits. Electronic structure of ideal $TiO_2(110), TiO_2(001)$, and $TiO_2(100)$ surfaces. *Phys. Rev. B*, 30(4):2202–2211, 1984.

[63] A. Nakano, M.E. Bachlechner, T.J. Campbell, A. Kalia, R.K.and Omeltchenko, K. Tsuruta, P. Vashishta, S. Ogata, I. Ebbsjö, and A. Madhukar. Atomistic simulation of nanostructured materials. *IEEE Computational Science & Engineering*, Oct–Dec:68–78, 1998.

[64] A. Neckel, K. Schwarz, R. Eibler, and P. Rastl. Bandstruktur des Festkörpers - Interpretation der chemischen Bindung in einigen Übergangsmetallverbindungen aufgrund von Bandstrukturrechnungen. *Berichte der Bunsengesellschaft*, 79(11):1053–1063, 1975.

[65] D.A. Papaconstantopoulos. *Handbook of the band structure of elemental solids*. Plenum Press, New York and London, 1986.

[66] D.A. Papaconstantopoulos, M.J. Mehl, S.C. Erwin, and M.R. Pderson. Tight-binding hamiltonians for carbon and silicon.

[67] A.D. Pearson. *J. Phys. Chem. Solids*, 5:316, 1958.

[68] F.L. Pilar. *Elementary quantum chemistry*. McGraw-Hill Book Company, 1968.

[69] D. Porezag, Th. Frauenheim, Th. Köhler, G. Seifert, and Th. Kaschner. Construction of tight-binding-like potentials on the basis of density-functional theory: Application to carbon. *Phys. Rev. B*, 51(19):12947–12957, 1995.

[70] D. Porezag, G. Jungnickel, Th. Frauenheim, G. Seifert, A. Ayuela, and M.R. Pederson. Theoretical investigations of homo- and heteronuclear bridged fullerene oligomers. *Appl. Phys. A*, 64:321–326, 1997.

[71] W.H. Press, S.A. Teukolsky, W.T. Vetterling, and B.P. Flannery. *Numerical recipes: the art of scientific computing.* Cambridge University Press, 1989.

[72] C. Salustri. Parametrisation of the band structure of FCC crystals. *Comp. Phys. Comm.*, 30:271–275, 1983.

[73] K.L. Shaklee and R.E. Nahory. Valley-orbit splitting of free exitons? the absorption edge of si. *Phys. Rev. Lett.*, 24(17):942–945, 1970.

[74] R.W. Siegel. Nanostructured materials: Mind over matter. *Nanostructured Materials*, 3:1–18, 1993.

[75] M.M. Sigalas and D.A. Papaconstantopoulos. Transferable total-energy parametrization for metals: applications to elastic-constant determination. *Phys. Rev. B*, 49(3), 1994.

[76] R.N. Silver and Röder, H. Densities of states of mega-dimensional hamiltonian matrices. *International Journal of Modern Physics C*, 5(4):735–753, 1994.

[77] R.N. Silver, Röder, H., A.F. Voter, and J.D. Kress. Kernel polynomial approximations for densities of states and spectral functions. *J. Comp. Phys.*, 124:115–130, 1996.

[78] C. Simmerling. Moil-view. http://morita.chem.sunysb.edu/ carlos/moil-view.html.

[79] J.C. Slater and G.F. Koster. Simplified LCAO method for the periodic potential problem. *Phys. Rev.*, 94(6):1498–1524, 1954.

[80] W.E. Spicer and R. Eden. *Proceedings of the ninth international conference of the physics of semiconductors*, 1:61–, 1968.

[81] M.G. Stachiotti, F. Coà, C.R.A. Catlow, and C.O. Rodrigues. First-principles investigation of ReO_3 and related oxides. *Phys. Rev. B*, 55(12):7508–7514, 1997.

[82] F. Starrost. Bestimmung von EHT-Parametern aus Bandstrukturen und Zustandsdichten mit vorwärtsgerichteten neuronalen Netzen. Master's thesis, Christian-Albrechts-Universität zu Kiel, 1994.

[83] F. Starrost, S. Bornholdt, C. Solterbeck, and W. Schattke. Band-structure parameters by genetic algorithm. *Phys. Rev. B*, 53(19):12549–12552, 1996.

[84] A.P. Sutton. *Elektronische Struktur in Materialien*. VCH, 1996.

[85] A.P. Sutton, M.W. Finnis, D.G. Pettifor, and Y. Ohta. The tight-binding bond model. *J. Phys. C: Solid State Phys.*, 21:35–66, 1988.

[86] H. Szu and R. Hartley. Fast simulated annealing. *Phys. Lett. A*, 122(3-4):157–162, 1987.

[87] G.K.M. Thutupalli and S.G. Tomlin. The optical properties of amorphous and crystalline silicon. *J. Phys. C: Solid State Phys.*, 10:467–477, 1977.

[88] K. Vos. Reflectance and electroreflectance of TiO_2 single crystals II: assignment to electronic energy levels. *J. Phys. C: Solid State Phys.*, 10:3917–3939, 1977.

[89] T. Wolfram. Two-dimensional character of the conduction bands of d-band perovskites. *Phys. Rev. Lett.*, 29(20):1383, 1972.

[90] S.H. Yang, M.J. Mehl, and D.A. Papaconstantopoulos. Application of a tight-binding total-energy method for Al, Ga, and In. *Phys. Rev. B Rapid Communications*, 57(4):R2013–R2016, 1998.